Diagnostic accuracy of optical flow ratio: an individual patient data meta-analysis

Fukang Hu[1], BSc; Daixin Ding[2], MSc; Jelmer Westra[3], MD, PhD; Yingguang Li[4], PhD; Wei Yu[1], PhD; Zhiqing Wang[5], MD; Takashi Kubo[6], MD, PhD; Juan Luis Gutiérrez-Chico[7], MD, PhD; Yundai Chen[8], MD, PhD; William Wijns[2], MD, PhD; Shengxian Tu[1]*, PhD

1. Biomedical Instrument Institute, School of Biomedical Engineering, Shanghai Jiao Tong University, Shanghai, People's Republic of China; 2. The Lambe Institute for Translational Research, Smart Sensors Laboratory and CURAM, University of Galway, Galway, Ireland; 3. Department of Cardiology, Aarhus University Hospital, Aarhus, Denmark; 4. Kunshan Industrial Technology Research Institute, Suzhou, People's Republic of China; 5. Department of Cardiology, Fujian Medical University Union Hospital, Fujian, China; 6. Department of Cardiovascular Medicine, Wakayama Medical University, Wakayama, Japan; 7. Department of Interventional Cardiology, Campo de Gibraltar Health Trust, Algeciras, Spain; 8. Department of Cardiology, Chinese PLA General Hospital, Beijing, People's Republic of China

F. Hu and D. Ding contributed equally to this work.

This paper also includes supplementary data published online at: https://eurointervention.pcronline.com/doi/10.4244/EIJ-D-22-01098

KEYWORDS

- ACS/NSTE-ACS
- fractional flow reserve
- optical coherence tomography
- stable angina

Abstract

Background: Optical flow ratio (OFR) is a novel method for the fast computation of fractional flow reserve (FFR) from optical coherence tomography.

Aims: We aimed to evaluate the diagnostic accuracy of OFR in assessing intermediate coronary stenosis using wire-based FFR as the reference.

Methods: We performed an individual patient-level meta-analysis of all available studies with paired OFR and FFR assessments. The primary outcome was vessel-level diagnostic concordance of the OFR and FFR, using a cut-off of ≤0.80 to define ischaemia and ≤0.90 to define suboptimal post-percutaneous coronary intervention (PCI) physiology. This meta-analysis was registered in PROSPERO (CRD42021287726).

Results: Five studies were finally included, providing 574 patients and 626 vessels (404 pre-PCI and 222 post-PCI) with paired OFR and FFR from 9 international centres. Vessel-level diagnostic concordance of the OFR and FFR was 91% (95% confidence interval [CI]: 88%-94%), 87% (95% CI: 82%-91%), and 90% (95% CI: 87%-92%) in pre-PCI, post-PCI, and overall, respectively. The overall sensitivity, specificity, and positive and negative predictive values were 84% (95% CI: 79%-88%), 94% (95% CI: 92%-96%), 90% (95% CI: 86%-93%), and 89% (95% CI: 86%-92%), respectively. Multivariate logistic regression indicated that a low pullback speed (odds ratio [OR] 7.02, 95% CI: 1.68-29.43; p=0.008) was associated with a higher risk of obtaining OFR values at least 0.10 higher than FFR. Increasing the minimal lumen area was associated with a lower risk of obtaining an OFR at least 0.10 lower than FFR (OR 0.39, 95% CI: 0.18-0.82; p=0.013).

Conclusions: This individual patient data meta-analysis demonstrated a high diagnostic accuracy of OFR. OFR has the potential to provide an improved integration of intracoronary imaging and physiological assessment for the accurate evaluation of coronary artery disease.

*Corresponding author: Biomedical Instrument Institute, School of Biomedical Engineering, Room123, Med-X Research Institute, Shanghai Jiao Tong University, No. 1954, Hua Shan Road, Xuhui District, Shanghai 200030, People's Republic of China. E-mail: sxtu@sjtu.edu.cn

Abbreviations

AUC	area under the curve
BMI	body mass index
CAD	coronary artery disease
FFR	fractional flow reserve
HSROC	hierarchical summary of receiver-operator characteristic curve
IPD	individual patient data
LAD	left anterior descending artery
MI	myocardial infarction
MLA	minimal lumen area
OCT	optical coherence tomography
OFR	optical flow ratio
OR	odds ratio
PCI	percutaneous coronary intervention
QFR	quantitative flow ratio

Introduction

Intracoronary optical coherence tomography (OCT) imaging provides super resolution *in vivo*, allowing detailed evaluation of coronary lumen, plaque characteristics, and stent expansion and apposition[1]. Fractional flow reserve (FFR) is the current reference standard for the functional evaluation of coronary artery stenosis[2]. An OCT-based morpho-functional evaluation approach based on a single catheter could reduce procedural complexity, time and cost, while enabling the use of both coronary imaging and physiology for percutaneous coronary intervention (PCI) guidance and optimisation.

Recently, a novel method for the fast computation of FFR from OCT images, optical flow ratio (OFR), has been developed[3]. The diagnostic performance of the OFR has been validated in *de novo* lesions, in-stent restenosis and native lesions immediately after PCI[3-7].

In this systematic, individual patient data (IPD) meta-analysis, we aimed to evaluate the diagnostic performance of the CE (European conformity)-marked OFR algorithm (Pulse Medical) with wire-based FFR as the reference standard.

Methods

Study selection, data extraction, analysis strategy, and data reporting were performed according to the PRIMSA guidelines for IPD meta-analysis. The authors of all the included studies were contacted for patient-level data for this IPD meta-analysis. This meta-analysis was registered in PROSPERO (CRD42021287726).

SEARCH STRATEGY

PubMed, Medline and Embase were searched for eligible studies using a combination of keywords including "optical coherence tomography", "optical flow ratio" and "fractional flow reserve". We applied no restrictions on language or publication period. A detailed search strategy is listed in **Supplementary Table 1**. The literature search was performed on 1 May 2022.

ELIGIBILITY CRITERIA

Prospective and retrospective studies with paired assessments of the OFR and wire-based FFR in patients with coronary artery disease (CAD), including both chronic and acute coronary syndromes, were considered. An additional criterion for eligibility was the use of the same CE-marked OFR algorithm, ensuring that the potential interstudy variation was not explained by software-related aspects. Duplicates, case reports, editorials, reviews or meta-analyses, and personal communications were excluded. Two independent observers performed the initial duplicate removal, screened the titles and abstracts, selected eligible studies following full text reviews, extracted the data, and performed quality scoring. Discrepancies were resolved by the involvement of a third reviewer.

DATA INTEGRITY

The data were double-checked for data integrity and correspondence with the individual published papers for key results related to completeness, accuracy and consistency. The reproduced results were confirmed by each study's principal author before data pooling.

RISK OF BIAS IN INDIVIDUAL STUDIES

The QUADAS-2 (Bristol University) system was used to assess the applicability and bias for each of the included studies.

ETHICS

All sites obtained approval from local institutional review boards for the individual studies. Written informed consent was provided by the patients or waived by the institutional review boards as appropriate.

OUTCOME MEASURES

The primary outcome was the vessel-level diagnostic concordance of OFR with wire-based FFR as reference standard in the overall population. Secondary outcome measures included vessel-level numerical agreement between OFR and FFR in the overall population: sensitivity, specificity, negative predictive value (NPV), positive predictive value (PPV), positive likelihood ratio (LR+), negative likelihood ratio (LR-) and a hierarchical summary of receiver-operator characteristics curve (HSROC) for OFR to predict wire-based FFR in the overall population. They also included identification of independent predictors for increased OFR–FFR difference using predefined clinical and lesion characteristics: age, sex, body mass index (BMI), hypertension, hyperlipidaemia, current smoker, diabetes, minimal lumen area (MLA), left anterior descending artery (LAD) lesion location, a high frame rate (100 frames/s classified as a low frame rate, while 180 frames/s classified as a high frame rate), a low pullback speed (18 mm/s and 20 mm/s classified as a low pullback speed while 36 mm/s classified as a high pullback speed), previous myocardial infarction (MI) and previous PCI.

OCT IMAGING

Details of OCT measurements were reported in all included studies[3-7]. In summary, OCT imaging was performed using

frequency-domain (FD) OCT systems (ILUMIEN, OPTIS, or C7-XR; Abbott), with the Dragonfly or Dragonfly Duo (also Abbott) imaging catheters, or the FD-OCT OPTIS system (LightLab Imaging) with the Dragonfly Duo and Dragonfly OPTIS catheter (Abbott). The fibre probe was pulled back at 18 mm/s, 20 mm/s or 36 mm/s within the stationary imaging sheath. Cross-sectional images were generated at a rotational speed of 100 frames/s or 180 frames/s. The cases from one centre were acquired with an F-1 system and a T-1 catheter (Forssmann Medical Co. Ltd.,), both with analogous technical characteristics to the above-mentioned system except for a rotation speed of 100 frames/s and a pullback speed of 18 mm/s.

OFR ANALYSIS

In all included studies, OFR analyses were performed by certified OFR analysts, blinded to clinical data and FFR values. OFR values at the distal position of the analysed vessel were obtained for comparison with wire-based FFR[3-7]. OFR analyses for vessels with *de novo* lesions, in-stent restenosis, and native vessels immediately after stenting were all included for evaluation of the primary and secondary outcome measures. A representative case example of OFR analysis is shown in the **Central illustration** and **Moving image 1**.

STATISTICAL ANALYSIS

Both one-stage and two-stage approaches (if applicable) were applied for this IPD meta-analysis. The one-stage approach analysed the IPD from all included studies in a single step, using a nested random-effect model accounting for study-level, centre-level, and patient-level clustering and heterogeneity. In the two-stage approach, first the IPD were used to obtain aggregate data (e.g., diagnostic performance of OFR against FFR) for each study separately, and second, these aggregate data were combined using a random-effect inverse variance-weighted meta-analysis. For the sake of succinctness, results derived from the one-stage approach were mainly presented throughout the manuscript, while results derived from the two-stage approach were presented in the **Supplementary data**. The diagnostic performance of OFR against FFR was analysed on a per-vessel level and repeated on a per-patient level to explore the effect of multivessel disease. In patients with paired OFR and FFR interrogated in multiple vessels, the vessel with the lowest FFR value with the corresponding OFR value was used. All analyses were performed for the overall population (pre- and post-PCI vessels combined), and then for pre-PCI vessels only and post-PCI vessels only, separately. For vessels before PCI, the diagnostic accuracy of the OFR was defined as the proportion of vessels with both OFR and FFR values of 0.80 or >0.80, while the cut-off value of 0.90 was used for both OFR and FFR in vessels immediately after PCI to identify physiologically suboptimal stenting results. A concordance correlation coefficient was used for evaluation of the correlation between FFR and OFR. Bland-Altman plots together with scatter plots were used to show the distribution of FFR and OFR. Subgroup analyses were performed regarding the numerical difference between OFR

and FFR, including pre-PCI versus post-PCI vessels, and European/American versus Asian centres. Univariate and multivariate logistic regression analyses were used to identify the potential clinical and procedural characteristics that were associated with OFR values that deviated from FFR values by at least 0.10. Potential publication bias was tested using Deek's funnel-plot asymmetry test for the main analysis. All analyses were performed by using MedCalc version 20 (MedCalc) and STATA version 14 (StataCorp). A two-sided p-value of <0.05 was considered statistically significant.

Results

STUDY SELECTION

Supplementary Figure 1 summarises the study flow. A total of 16 studies were identified with 10 of the studies entering title and abstract screening after the removal of duplicates. Finally, 7 articles were selected for full text review, of which 5 were included in the analysis. All 5 studies provided individual patient data. The studies showed high methodological quality with low risk of bias rated by QUADAS-2 **(Supplementary Figure 2)**.

STUDY AND PATIENT CHARACTERISTICS

The main findings of all the included studies are listed in **Table 1**. Baseline clinical and lesion characteristics of a total of 574 patients with 626 vessels are listed in **Table 2**. Among them, paired pre-PCI OFR and FFR was available in 404 vessels with *de novo* lesions or in-stent restenosis, while paired post-PCI OFR and FFR was available in the remaining 222 vessels. The median vessel-level FFR was 0.86 (0.79-0.93) in the overall population, 0.83 (0.76-0.89) in vessels with *de novo* lesions or in-stent restenosis, and 0.92 (0.88-0.96) in vessels post-PCI. A total of 171 (42.3%) vessels with paired pre-PCI measurements were physiologically significant as identified by FFR ≤0.80. A total of 85 (38.3%) vessels with paired post-PCI measurements were physiologically suboptimal as identified by post-PCI FFR ≤0.90. Deek's funnel plot asymmetry test **(Supplementary Figure 3)** showed that there was no significant publication bias (p=0.64).

CORRELATION AND AGREEMENT BETWEEN OFR AND FFR

The overall vessel-level concordance correlation coefficient between OFR and FFR was 0.86 (95% CI: 0.84-0.88) **(Supplementary Table 2)**, showing increased scatter along with lower FFR values **(Supplementary Figure 4)**. The pooled vessel-level mean difference of OFR and FFR in the overall population was 0.002±0.05 with heterogeneity of I^2=0.0% **(Supplementary Figure 5)**. The vessel-level numerical agreement of OFR and FFR was independent of baseline clinical parameters and centre region **(Figure 1, Supplementary Figure 6)**. The vessel-level concordance correlation coefficient and pooled mean difference of OFR and FFR were further tested in pre-PCI and post-PCI vessels separately, with results shown in **Supplementary Table 2** and **Supplementary Figure 4-Supplementary Figure 8**. Sensitivity analysis showed that the numerical difference of OFR and FFR was not influenced by the removal of each of the 5 studies **(Supplementary Table 3)**.

CENTRAL ILLUSTRATION A representative case example of OFR analysis.
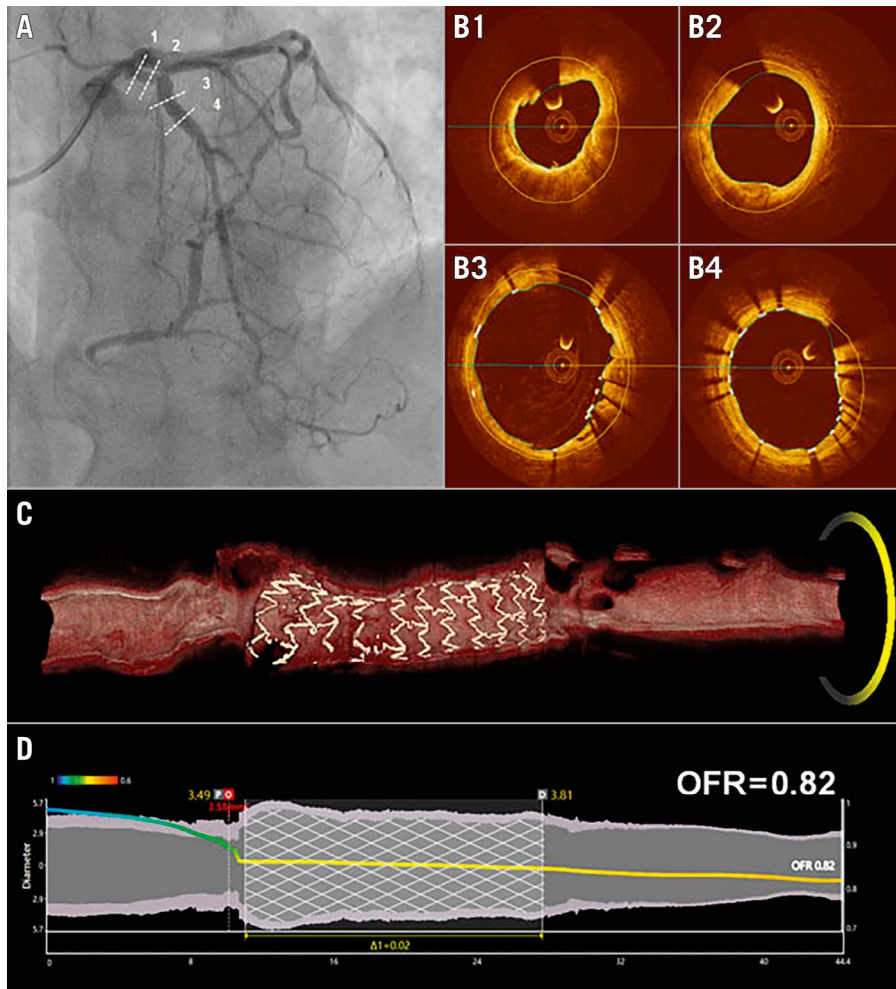
A) Coronary angiography immediately after PCI for a lesion mid-LAD. B1-B4) Correspond to the four positions (dashed lines) in (A). C) 3D reconstruction of both the lumen and stent struts from OCT pullback image. D) Co-registration between OFR pullback curve and lumen diameters for the reconstructed vessel. 3D: three-dimensional; LAD: left anterior descending artery; OCT: optical coherence tomography; OFR: optical flow ratio; PCI: percutaneous coronary intervention

Table 1. Study characteristics.

Study	Patients (vessels)	Median FFR	FFR ≤0.80	FFR ≤0.90	Correlation	SD	Accuracy, % (95% CI)	AUC (95% CI)
Yu et al[3]	118 (125)	0.80 (0.79-0.82)	50.4%	86.4%	0.70	0.07	90 (84-95)	0.93 (0.87-0.97)
Huang et al[4]	181 (212)	0.83 (0.81-0.85)	40.1%	75.0%	0.87	0.05	92 (88-95)	0.97 (0.93-0.99)
Gutiérrez-Chico et al[5]	53 (67)	0.84 (0.82-0.86)	34.3%	79.1%	0.82	0.05	93 (86-99)	0.95 (0.86-0.99)
Emori et al[6]	103 (103)	0.91 (0.89-0.93)	7.8%	52.4%	0.84	0.02	90 (82-95)	0.90 (0.83-0.95)
Ding et al[7]	119 (119)	0.94 (0.92-0.95)	3.4%	26.1%	0.80	0.04	84 (77-91)	0.89 (0.82-0.94)
AUC: area under the curve; CI: confidence interval; FFR: fractional flow reserve; SD: standard deviation								

OFR DISTRIBUTION ACCORDING TO FFR RANGES

The distribution of OFR data according to different ranges of FFR values is shown in **Supplementary Figure 9**. The majority of OFR observations were located in the FFR range 0.60 to 0.90.

DIAGNOSTIC ACCURACY OF OFR

The overall vessel-level diagnostic concordance of OFR and FFR was 90% (95% confidence interval [CI]: 87%-92%) in the overall population, using a cut-off value of 0.80 in pre-PCI vessels

Table 2. Baseline clinical and lesion characteristics.

Patients (n=574)		
Demographics	Age, years	69.5±2
	Female	115 (20%)
	BMI, kg/m^2	25.1±0.5
Risk factors	Hypertension	451 (79%)
	Hyperlipidaemia	370 (64%)
	Diabetes mellitus	206 (36%)
	Current smoker	148 (26%)
Cardiac history	Previous PCI	251 (44%)
	Previous CABG	8 (1%)
	Previous MI	196 (34%)
	Family history of CAD	79 (14%)
Clinical presentation	Stable angina	227 (40%)
	Unstable angina	76 (13%)
	Silent ischaemia	132 (23%)
	Other (including NSTEMI)	139 (24%)
Vessels (n=626)		
Interrogated vessels	Left anterior descending artery	371 (59%)
	Diagonal branch	5 (1%)
	Left circumflex artery	100 (16%)
	Obtuse marginal branch	4 (1%)
	Ramus intermedius	2 (0.3%)
	Right coronary artery	144 (23%)
FFR	Mean±standard deviation	0.85±0.10
	Median (quartiles)	0.86 (0.79-0.93)

Values are presented as n (%), mean±standard deviation, or median (quartiles). BMI: body mass index; CABG: coronary artery bypass surgery; CAD: coronary artery disease; FFR: fractional flow reserve; MI: myocardial infarction; NSTEMI: non-ST-segment elevation myocardial infarction; PCI: percutaneous coronary intervention

and a cut-off value of 0.90 in post-PCI vessels **(Supplementary Table 4, Supplementary Table 5)**. The pooled diagnostic performance estimates in the overall population were as follows: sensitivity 84% (95% CI: 79%-88%), specificity 94% (95% CI: 91%-96%), positive predictive value 90% (95% CI: 86%-93%), negative predictive value 89% (95% CI: 86%-92%), positive likelihood ratio 13.51 (95% CI: 9.06-20.14), and negative likelihood ratio 0.17 (95% CI: 0.13-0.23). The diagnostic concordance of OFR and FFR was 91% (95% CI: 88%-94%) in pre-PCI vessels, and 87% (95% CI: 82%-91%) in post-PCI vessels. Other diagnostic measures in both pre- and post-PCI data are shown in **Supplementary Table 5**. The forest plot results by two-stage analyses are illustrated in **Supplementary Figure 10-Supplementary Figure 15**. HSROC curves for vessel- and patient-level data separately are shown in **Supplementary Figure 16** and **Supplementary Figure 17**.

PATIENT-LEVEL ANALYSIS

At the patient-level, the diagnostic concordance of OFR and FFR was 90% (95% CI: 87%-92%) in the overall population, 91%

(95% CI: 88%-94%) in pre-PCI vessels, and 87% (95% CI: 82%-91%) in post-PCI vessels. Other patient-level diagnostic performance estimates are listed in **Supplementary Table 6**.
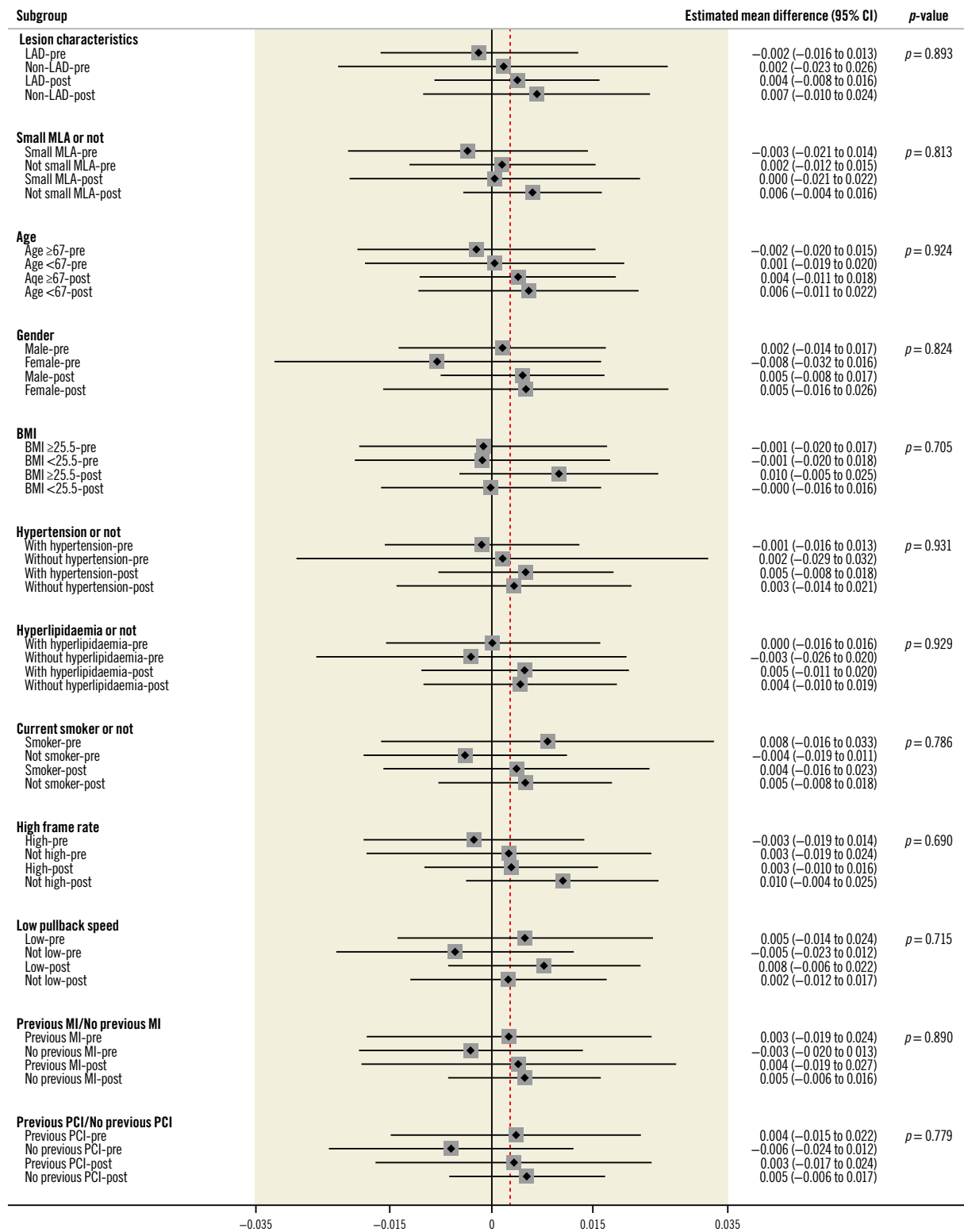
PREDICTION OF OFR–FFR DISAGREEMENT

In the overall population, multivariate regression analyses demonstrated that the MLA was an independent predictor of an OFR ≥0.10 lower than FFR (odds ratio [OR] 0.39, 95% CI: 0.18-0.82; p=0.013) and a low pullback speed (OR 7.02, 95% CI: 1.68-29.43; p=0.008) was an independent predictor of OFR ≥0.10 higher than FFR **(Table 3, Table 4)**. Multivariate regression analyses were repeated in pre-PCI vessels only and a low pullback speed was an independent predictor of an OFR ≥0.10 higher than FFR **(Table 3, Table 4)**. The distribution of cases with OFR−FFR ≥0.10 or OFR−FFR ≤−0.10 stratified by ranges of FFR values is listed in **Supplementary Table 7**. In post-PCI vessels, stent length was not significantly associated with OFR−FFR ≥0.10 (OR 0.92, 95% CI: 0.70-1.22; p=0.566) or OFR−FFR ≤–0.10 (OR 0.79, 95% CI: 0.50-1.12; p=0.297) by univariate regression analysis.

Discussion

The following points summarise the main findings of the present study: (1) OFR had a high diagnostic accuracy with wire-based FFR; (2) there was good correlation and numerical agreement between the OFR and FFR, with increased scatter along with lower FFR values; (3) centre-level data analysis revealed that the agreement between OFR and FFR was independent of geography, and (4) OCT-derived low MLA and low pullback speed were independent predictors of an increased numerical difference (>0.10) between OFR and FFR.

The overall good correlation and numerical agreement between OFR and FFR can be attributed to the following factors. The novel algorithm of computational FFR[8] was applied to the OCT images with super *in vivo* resolution, which provided precise lumen dimensions as the geometric boundary[3]. Instead of using a linear tapering reference lumen, the area of the side branch ostium was used to compute a step-down reference vessel function across bifurcations[3]. This provided a more accurate reconstruction of the normal coronary lumen and an estimation of downstream blood flow. In the presence of implanted stents, all struts were detected and reconstructed in 3D using a deep learning-based algorithm[9], incorporated with lumen geometry for pressure drop computation. The described approach produced a pressure pullback curve along the reconstructed vessel allowing for differentiation of diffuse and focal disease **(Central illustration)**.

To combine physiological and morphological assessments using a single OCT catheter, several similar concepts have been previously proposed[10-13], with most models predominantly relying on computational fluid dynamics and having the inherent limitations of a long computational time[12]. Recently, Seike et al developed a new approach based on fluid dynamics equations and shortened the computational time to 10 minutes[11]. However, only

Subgroup	Estimated mean difference (95% CI)	*p*-value
Lesion characteristics		
LAD-pre	−0.002 (−0.016 to 0.013)	*p* = 0.893
Non-LAD-pre	0.002 (−0.023 to 0.026)	
LAD-post	0.004 (−0.008 to 0.016)	
Non-LAD-post	0.007 (−0.010 to 0.024)	
Small MLA or not		
Small MLA-pre	−0.003 (−0.021 to 0.014)	*p* = 0.813
Not small MLA-pre	0.002 (−0.012 to 0.015)	
Small MLA-post	0.000 (−0.021 to 0.022)	
Not small MLA-post	0.006 (−0.004 to 0.016)	
Age		
Age ≥67-pre	−0.002 (−0.020 to 0.015)	*p* = 0.924
Age <67-pre	0.001 (−0.019 to 0.020)	
Age ≥67-post	0.004 (−0.011 to 0.018)	
Age <67-post	0.006 (−0.011 to 0.022)	
Gender		
Male-pre	0.002 (−0.014 to 0.017)	*p* = 0.824
Female-pre	−0.008 (−0.032 to 0.016)	
Male-post	0.005 (−0.008 to 0.017)	
Female-post	0.005 (−0.016 to 0.026)	
BMI		
BMI ≥25.5-pre	−0.001 (−0.020 to 0.017)	*p* = 0.705
BMI <25.5-pre	−0.001 (−0.020 to 0.018)	
BMI ≥25.5-post	0.010 (−0.005 to 0.025)	
BMI <25.5-post	−0.000 (−0.016 to 0.016)	
Hypertension or not		
With hypertension-pre	−0.001 (−0.016 to 0.013)	*p* = 0.931
Without hypertension-pre	0.002 (−0.029 to 0.032)	
With hypertension-post	0.005 (−0.008 to 0.018)	
Without hypertension-post	0.003 (−0.014 to 0.021)	
Hyperlipidaemia or not		
With hyperlipidaemia-pre	0.000 (−0.016 to 0.016)	*p* = 0.929
Without hyperlipidaemia-pre	−0.003 (−0.026 to 0.020)	
With hyperlipidaemia-post	0.005 (−0.011 to 0.020)	
Without hyperlipidaemia-post	0.004 (−0.010 to 0.019)	
Current smoker or not		
Smoker-pre	0.008 (−0.016 to 0.033)	*p* = 0.786
Not smoker-pre	−0.004 (−0.019 to 0.011)	
Smoker-post	0.004 (−0.016 to 0.023)	
Not smoker-post	0.005 (−0.008 to 0.018)	
High frame rate		
High-pre	−0.003 (−0.019 to 0.014)	*p* = 0.690
Not high-pre	0.003 (−0.019 to 0.024)	
High-post	0.003 (−0.010 to 0.016)	
Not high-post	0.010 (−0.004 to 0.025)	
Low pullback speed		
Low-pre	0.005 (−0.014 to 0.024)	*p* = 0.715
Not low-pre	−0.005 (−0.023 to 0.012)	
Low-post	0.008 (−0.006 to 0.022)	
Not low-post	0.002 (−0.012 to 0.017)	
Previous MI/No previous MI		
Previous MI-pre	0.003 (−0.019 to 0.024)	*p* = 0.890
No previous MI-pre	−0.003 (−0.020 to 0.013)	
Previous MI-post	0.004 (−0.019 to 0.027)	
No previous MI-post	0.005 (−0.006 to 0.016)	
Previous PCI/No previous PCI		
Previous PCI-pre	0.004 (−0.015 to 0.022)	*p* = 0.779
No previous PCI-pre	−0.006 (−0.024 to 0.012)	
Previous PCI-post	0.003 (−0.017 to 0.024)	
No previous PCI-post	0.005 (−0.006 to 0.017)	

Axis: −0.035   −0.015   0   0.015   0.035

Figure 1. *Subgroup analysis, presented as the numerical difference between OFR and FFR by vessel level. Small MLA ≤1.88 mm² for pre-PCI[4] and small MLA ≤3.28 mm² for post-PCI[7]. BMI: body mass index; CI: confidence interval; FFR: fractional flow reserve; LAD: left anterior descending artery; MI: myocardial infarction; MLA: minimal lumen area; OFR: optical flow ratio; PCI: percutaneous coronary intervention*

single-vessel models are used, while the fractal flow in bifurcations was not taken into account. Sufficient clinical validations for the above-mentioned methods are still lacking. OFR has emerged as an appealing tool in simultaneous physiological and morphological assessments, given the fast computational time of around 1 minute[3] and high overall diagnostic accuracy of 90%.

Table 3. Predictors of OFR−FFR ≥0.10 by univariate and multivariate analyses at the vessel-level.

Variables*	Predictors of OFR−FFR ≥0.10							
	Pre-PCI				Combined			
	Univariate regression		Multivariate regression		Univariate regression		Multivariate regression	
	OR (95% CI)	*p*-value	OR (95% CI)	*p*-value	OR (95% CI)	*p*-value	OR (95% CI)	*p*-value
Age	1.00 (0.95-1.04)	0.998	1.02 (0.97-1.08)	0.392	1.00 (0.95-1.04)	0.858	1.01 (0.96-1.07)	0.619
Gender	2.01 (0.55-7.27)	0.288	1.60 (0.40-6.42)	0.511	2.00 (0.55-7.22)	0.292	1.83 (0.46-7.22)	0.389
BMI	1.01 (0.92-1.11)	0.845	1.00 (0.89-1.12)	0.985	1.00 (0.91-1.09)	0.898	0.99 (0.88-1.10)	0.814
Hypertension	1.03 (0.28-3.79)	0.970	0.91 (0.21-4.01)	0.903	0.82 (0.25-2.68)	0.743	0.75 (0.20-2.84)	0.673
Hyperlipidaemia	1.74 (0.54-5.64)	0.358	1.27 (0.35-4.58)	0.718	1.38 (0.47-4.08)	0.563	1.18 (0.35-3.98)	0.791
Current smoker	2.87 (1.06-7.81)	0.038	2.96 (0.92-9.60)	0.069	2.47 (0.92-6.68)	0.074	2.28 (0.73-7.07)	0.155
Diabetes	1.70 (0.65-4.47)	0.281	1.69 (0.55-5.23)	0.362	1.59 (0.62-4.10)	0.334	1.58 (0.53-4.76)	0.415
MLA	1.17 (0.76-1.81)	0.475	1.11 (0.69-1.78)	0.664	0.87 (0.56-1.36)	0.535	0.81 (0.50-1.34)	0.419
LAD	0.52 (0.20-1.36)	0.182	0.54 (0.19-1.56)	0.256	0.47 (0.18-1.21)	0.118	0.49 (0.18-1.35)	0.168
High frame rate	1.49 (0.37-5.95)	0.575	3.87 (0.67-22.54)	0.132	1.76 (0.43-7.22)	0.434	4.40 (0.82-23.64)	0.084
Low pullback speed	2.29 (0.74-7.08)	0.150	5.41 (1.21-24.21)	0.027	2.56 (0.82-7.98)	0.105	7.02 (1.68-29.43)	0.008
Previous MI	2.23 (0.81-6.13)	0.119	1.79 (0.51-6.32)	0.365	2.14 (0.81-5.73)	0.126	1.54 (0.46-5.20)	0.486
Previous PCI	1.71 (0.58-5.04)	0.328	1.62 (0.38-6.95)	0.519	1.75 (0.62-4.92)	0.291	1.66 (0.42-6.62)	0.472

*Gender, hypertension, hyperlipidaemia, current smoker, diabetes, LAD, high frame rate, low pullback speed, previous MI and previous PCI were included as binary variables while the remaining were included as continuous variables. High frame rate=180 frame/s, low pullback speed=18 mm/s or 20 mm/s. BMI: body mass index; CI: confidence interval; FFR: fractional flow reserve; LAD: left anterior descending artery; MI: myocardial infarction; MLA: minimal lumen area; OFR: optical flow ratio; OR: odds ratio; PCI: percutaneous coronary intervention

Table 4. Predictors of OFR−FFR ≤−0.10 by univariate and multivariate analyses at vessel level.

Variables*	Predictors of OFR−FFR ≤−0.10							
	Pre-PCI				Combined			
	Univariate regression		Multivariate regression		Univariate regression		Multivariate regression	
	OR (95% CI)	*p*-value	OR (95% CI)	*p*-value	OR (95% CI)	*p*-value	OR (95% CI)	*p*-value
Age	1.00 (0.95-1.05)	0.962	0.98 (0.92-1.04)	0.485	0.98 (0.94-1.04)	0.544	0.96 (0.91-1.03)	0.250
Gender	1.01 (0.30-3.40)	0.993	1.27 (0.30-5.35)	0.747	0.90 (0.26-3.08)	0.866	1.10 (0.28-4.29)	0.897
BMI	1.01 (0.92-1.11)	0.886	0.99 (0.87-1.13)	0.900	0.99 (0.89-1.11)	0.910	0.99 (0.87-1.12)	0.820
Hypertension	1.45 (0.33-6.32)	0.620	1.83 (0.32-10.36)	0.496	1.24 (0.32-4.84)	0.754	1.21 (0.27-5.42)	0.801
Hyperlipidaemia	1.81 (0.54-6.01)	0.335	1.83 (0.45-7.34)	0.395	2.28 (0.65-7.98)	0.198	2.09 (0.55-7.96)	0.280
Current smoker	1.21 (0.37-3.95)	0.753	0.84 (0.20-3.42)	0.804	1.37 (0.42-4.50)	0.605	1.10 (0.31-3.92)	0.884
Diabetes	1.81 (0.64-5.14)	0.266	1.73 (0.50-5.99)	0.390	1.73 (0.61-4.91)	0.302	1.39 (0.44-4.36)	0.571
MLA	0.46 (0.21-1.01)	0.053	0.48 (0.20-1.18)	0.112	0.42 (0.22-0.79)	0.007	0.39 (0.18-0.82)	0.013
LAD	0.72 (0.24-2.17)	0.560	0.59 (0.17-2.05)	0.406	0.81 (0.28-2.34)	0.695	0.62 (0.19-1.98)	0.417
High frame rate	2.24 (0.53-9.50)	0.272	0.99 (0.06-16.11)	0.992	2.44 (0.47-12.80)	0.290	2.14 (0.22-21.10)	0.514
Low pullback speed	0.36 (0.09-1.45)	0.151	0.26 (0.02-3.94)	0.333	0.42 (0.11-1.64)	0.213	0.82 (0.12-5.82)	0.845
Previous MI	0.88 (0.30-2.60)	0.814	1.82 (0.33-10.12)	0.495	0.90 (0.29-2.80)	0.861	1.58 (0.32-7.83)	0.576
Previous PCI	0.45 (0.15-1.30)	0.140	0.16 (0.02-1.25)	0.081	0.44 (0.13-1.50)	0.190	0.21 (0.04-1.27)	0.090

*Gender, hypertension, hyperlipidaemia, current smoker, diabetes, LAD, high frame rate, low pullback speed, previous MI and previous PCI were included as binary variables while the remaining were included as continuous variables. High frame rate=180 frame/s, low pullback speed=18 mm/s or 20 mm/s. BMI: body mass index; CI: confidence interval; FFR: fractional flow reserve; LAD: left anterior descending artery; MI: myocardial infarction; MLA: minimal lumen area; OFR: optical flow ratio; OR: odds ratio; PCI: percutaneous coronary intervention

Most of the studies included in this meta-analysis applied OFR in addition to the angiography-based quantitative flow ratio (QFR)[8,14-16]. Fundamentally, both QFR and OFR adapt fluid dynamics equations for the estimation of FFR but with fundamental differences related to vessel geometry reconstruction and the estimated blood flow rate[3]. The lumen reconstruction related to OFR is more accurate than that of QFR given the resolution of intravascular imaging. However, compared with the QFR's reconstruction algorithm, including the estimation of hyperaemic flow based on contrast flow[8], OCT provides static images with no dynamic parameters available for flow velocity estimation. Specifically, in the OFR algorithm, patient-specific volumetric flow is derived from a fixed hyperaemic flow velocity of 0.35 m/s multiplied by the reference vessel size[17]. The combination of

a geometrical reconstruction based on high-resolution intravascular imaging and a fixed flow rate in the form of OFR appears to outperform QFR[4]. The presented bias and imprecision (standard deviation [SD]±0.05) are at a level not previously presented in similar populations for alternative solutions based on coronary computed tomography angiography (CTA) and invasive angiography[16,18]. More importantly, the minimal user interaction related to OFR measurements appears to have helped overcome a major limitation in terms of reproducibility for image-based physiology[19]. The test-retest repeatability of OFR approaches results from FFR reproducibility studies (SD of ±0.02 for intra-observer agreement)[3,20]. With the acceptance of QFR in a global scope, OFR may grow into a complementary solution in cases with the need for culprit or non-culprit plaque evaluation and for planning purposes in patients with an *a priori* high likelihood of PCI[4]. In post-PCI settings, OCT visualises coronary lumen, stent struts and plaque compositions in detail, providing the rationale for the evaluation of PCI efficacy and PCI optimisation[7]. Admittedly, in comparison with the QFR, limited outcome data exist validating the prognostic value of the OFR in either pre- or post-PCI scenarios. The only evidence comes from a recent study showing that OFR in combination with a novel morphological index, lipid-to-cap ratio (LCR), allows for the identification of a subgroup of patients with a 43-fold higher risk of recurrent cardiovascular events in non-culprit vessels after acute coronary syndromes[21]. Further prognostic data would help justify the clinical use of the OFR. In addition, the clinical application of the OFR naturally depends on the penetration of intracoronary imaging itself, which is still limited in many areas. However, computational approaches exist for a broad variety of imaging modalities, thus, also allowing for the use of intravascular ultrasound (IVUS) that could have advantages over OCT in specific patients and lesion types (e.g., ostial lesions)[16,22].

The current multicentre and multiregion clinical database provides robust diagnostic performance estimates informing on the reliability of OFR across Asian and US/EU regions. Our results apply to a broad range of patients (due to the inclusion of both stable angina and acute coronary syndrome) with mean FFR values in line with previous large all-comer invasive physiology studies[23]. Moreover, the results provide a foundation for the identification of factors affecting the accuracy of the OFR. Firstly, our results show that a high frame rate has limited influence on the OFR's accuracy, while a higher pullback speed appears to be favourable to reduce large differences between the OFR and FFR (>0.10). One of the possible explanations for the latter is that a lower pullback speed might be more subject to cardiac motion artefact. It increased the risk of longitudinal discontinuity between consecutive OCT frames, leading to inaccuracies in 3D lumen reconstruction and pressure drop computation. Secondly, an increase in the MLA decreases the risk of a large OFR−FFR difference (>0.10). The clinical importance of the reduced precision of computational FFR in severe stenoses is still not clear, since most of the tight stenoses would have been stented. However, more evidence is needed on the combined use of OCT and OFR in populations, including more severe lesions intended for PCI where the mean FFR is likely to approach 0.70[24].

Limitations

Although the sample size of this analysis is increased by meta-pooling, the proportion of prospective and retrospective studies is not balanced, with only one prospective study. As each included study has a different emphasis, not all potential factors of interest could be included in the current study (e.g., plaque composition, microcirculatory dysfunction, tandem lesions, diffuse disease). We were not able to perform a subgroup analysis according to lesion location (proximal/middle/distal) because such information was not reported by all the included publications. In all the included studies, the OFR values at the distal position of the analysed vessel were obtained for comparison with wire-based FFR. In clinical practice, OCT catheters are usually placed less distally than pressure wires[6]. Although vessels with stenosis between the positions of the distal optical sensor and pressure sensor had been excluded in all studies, a pressure drop might still be seen in certain non-stenotic but atherosclerotic vessels[25]. This could be a possible source of deviation of OFR values from FFR values. Future OCT imaging systems with faster pullback speeds and longer pullback lengths might reduce the discrepancy between the OFR and FFR. The heterogeneity index I^2 was high for several pooled estimates including sensitivity, mainly caused by a relatively different level of diagnostic estimates found by Ding et al[7] compared with the other 4 studies **(Supplementary Figure 10-Supplementary Figure 15)**. Of note, in post-PCI datasets, as enrolled by Ding et al[7], the OFR and FFR values showed a narrow range and skewed distribution towards normal values, with a mean FFR of 0.92 and a mean OFR of 0.93, which introduced a higher risk of finding false negative results[7]. Therefore, the overall high pooled estimates should be interpreted with caution that variation could exist in the diagnostic performance in populations with different levels of physiology. Nevertheless, the sensitivity analysis showed that the numerical difference of the OFR and FFR was not influenced by the removal of any of the 5 studies. Lastly, prognostic data of OFR are still limited, despite a recent study finding that OFR independently predicted non-culprit vessel related major adverse cardiovascular events at 2-year follow-up, with an area under the curve (AUC) of 0.838 (95% CI: 0.806-0.866)[21]. Thus, the good diagnostic concordance between OFR and FFR found in the current meta-analysis should be considered as only hypothesis-generating. Future studies investigating the prognostic value of OFR are warranted. It would also be interesting to explore the risk stratification function based on a combination of OFR and other factors including high-risk plaque features (e.g., thin cap, edge dissection, stent underexpansion, etc.) in a future study.

Conclusions

This meta-analysis based on individual patient data demonstrated high diagnostic accuracy for OFR using wire-based FFR as the reference. The OFR has the potential to provide an improved

integration of intracoronary imaging and physiological assessment for accurate evaluation of coronary artery disease in the catheterisation laboratory.

Impact on daily practice

The OFR enables functional and morphological assessment of coronary artery stenoses including an evaluation of stent expansion and apposition with the use of a single catheter. The increasing application of OCT has the potential to optimise coronary interventions.

Funding

Conflict of interest statement

S. Tu reports research grants from and is a consultant for Pulse Medical. W. Wijns reports institutional research grants and past honoraria from MicroPort; is a senior advisor of Rede Optimus Research and Corrib Core Laboratory; and is a co-founder of Argonauts, an innovation facilitator. The other authors have no conflicts of interest to declare.

References

1. Räber L, Mintz GS, Koskinas KC, Johnson TW, Holm NR, Onuma Y, Radu MD, Joner M, Yu B, Jia H, Meneveau N, de la Torre Hernandez JM, Escaned J, Hill J, Prati F, Colombo A, di Mario C, Regar E, Capodanno D, Wijns W, Byrne RA, Guagliumi G; ESC Scientific Document Group. Clinical use of intracoronary imaging. Part 1: guidance and optimization of coronary interventions. An expert consensus document of the European Association of Percutaneous Cardiovascular Interventions. Eur Heart J. 2018;39:3281-300.

2. Knuuti J, Wijns W, Saraste A, Capodanno D, Barbato E, Funck-Brentano C, Prescott E, Storey RF, Deaton C, Cuisset T, Agewall S, Dickstein K, Edvardsen T, Escaned J, Gersh BJ, Svitil P, Gilard M, Hasdai D, Hatala R, Mahfoud F, Masip J, Muneretto C, Valgimigli M, Achenbach S, Bax JJ; ESC Scientific Document Group. 2019 ESC Guidelines for the diagnosis and management of chronic coronary syndromes. Eur Heart J. 2020;41:407-77.

3. Yu W, Huang J, Jia D, Chen S, Raffel OC, Ding D, Tian F, Kan J, Zhang S, Yan F, Chen Y, Bezerra HG, Wijns W, Tu S. Diagnostic accuracy of intracoronary optical coherence tomography-derived fractional flow reserve for assessment of coronary stenosis severity. EuroIntervention. 2019;15:189-97.

4. Huang J, Emori H, Ding D, Kubo T, Yu W, Huang P, Zhang S, Gutiérrez-Chico JL, Akasaka T, Wijns W, Tu S. Diagnostic performance of intracoronary optical coherence tomography-based versus angiography-based fractional flow reserve for the evaluation of coronary lesions. EuroIntervention. 2020;16:568-76.

5. Gutiérrez-Chico JL, Chen Y, Yu W, Ding D, Huang J, Huang P, Jing J, Chu M, Wu P, Tian F, Xu B, Tu S. Diagnostic accuracy and reproducibility of optical flow ratio for functional evaluation of coronary stenosis in a prospective series. Cardiol J. 2020;27:350-61.

6. Emori H, Kubo T, Shiono Y, Ino Y, Shimamura K, Terada K, Nishi T, Higashioka D, Takahata M, Wada T, Kashiwagi M, Khalifa AKM, Tanaka A, Hozumi T, Tu S, Akasaka T. Comparison of Optical Flow Ratio and Fractional Flow Ratio in Stent-Treated Arteries Immediately After Percutaneous Coronary Intervention. Circ J. 2020; 84:2253-8.

7. Ding D, Yu W, Tauzin H, De Maria GL, Wu P, Yang F, Kotronias RA, Terentes-Printzios D, Wolfrum M, Banning AP, Meneveau N, Wijns W, Tu S. Optical flow ratio for assessing stenting result and physiological significance of residual disease. EuroIntervention. 2021;17:e989-98.

8. Tu S, Westra J, Yang J, von Birgelen C, Ferrara A, Pellicano M, Nef H, Tebaldi M, Murasato Y, Lansky A, Barbato E, van der Heijden LC, Reiber JHC, Holm NR,

Wijns W; FAVOR Pilot Trial Study Group. Diagnostic Accuracy of Fast Computational Approaches to Derive Fractional Flow Reserve From Diagnostic Coronary Angiography: The International Multicenter FAVOR Pilot Study. JACC Cardiovasc Interv. 2016;9:2024-35.

9. Wu P, Gutiérrez-Chico JL, Tauzin H, Yang W, Li Y, Yu W, Chu M, Guillon B, Bai J, Meneveau N, Wijns W, Tu S. Automatic stent reconstruction in optical coherence tomography based on a deep convolutional model. Biomed Opt Express. 2020;11: 3374-94.

10. Guagliumi G, Sirbu V, Petroff C, Capodanno D, Musumeci G, Yamamoto H, Elbasiony A, Brushett C, Matiashvili A, Lortkipanidze N, Valsecchi O, Bezerra HG, Schmitt JM. Volumetric assessment of lesion severity with optical coherence tomography: relationship with fractional flow. EuroIntervention. 2013;8:1172-81.

11. Seike F, Uetani T, Nishimura K, Kawakami H, Higashi H, Aono J, Nagai T, Inoue K, Suzuki J, Kawakami H, Okura T, Yasuda K, Higaki J, Ikeda S. Intracoronary Optical Coherence Tomography-Derived Virtual Fractional Flow Reserve for the Assessment of Coronary Artery Disease. Am J Cardiol. 2017;120:1772-9.

12. Ha J, Kim JS, Lim J, Kim G, Lee S, Lee JS, Shin DH, Kim BK, Ko YG, Choi D, Jang Y, Hong MK. Assessing Computational Fractional Flow Reserve From Optical Coherence Tomography in Patients With Intermediate Coronary Stenosis in the Left Anterior Descending Artery. Circ Cardiovasc Interv. 2016;9:e003613.

13. Lee KE, Lee SH, Shin E-S, Shim EB. A vessel length-based method to compute coronary fractional flow reserve from optical coherence tomography images. BioMed Eng Online. 2017;16:83.

14. Xu B, Tu S, Qiao S, Qu X, Chen Y, Yang J, Guo L, Sun Z, Li Z, Tian F, Fang W, Chen J, Li W, Guan C, Holm NR, Wijns W, Hu S. Diagnostic Accuracy of Angiography-Based Quantitative Flow Ratio Measurements for Online Assessment of Coronary Stenosis. J Am Coll Cardiol. 2017;70:3077-87.

15. Westra J, Tu S, Winther S, Nissen L, Vestergaard MB, Andersen BK, Holck EN, Fox Maule C, Johansen JK, Andreasen LN, Simonsen JK, Zhang Y, Kristensen SD, Maeng M, Kaltoft A, Terkelsen CJ, Krusell LR, Jakobsen L, Reiber JHC, Lassen JF, Bottcher M, Botker HE, Christiansen EH, Holm NR. Evaluation of Coronary Artery Stenosis by Quantitative Flow Ratio During Invasive Coronary Angiography: The WIFI II Study (Wire-Free Functional Imaging II). Circ Cardiovasc Imaging. 2018;11: e007107.

16. Tu S, Westra J, Adjedj J, Ding D, Liang F, Xu B, Holm NR, Reiber JHC, Wijns W. Fractional flow reserve in clinical practice: From wire-based invasive measurement to image-based computation. Eur Heart J. 2020;41:3271-9.

17. Tu S, Echavarria-Pinto M, von Birgelen C, Holm NR, Pyxaras SA, Kumsars I, Lam MK, Valkenburg I, Toth GG, Li Y, Escaned J, Wijns W, Reiber JH. Fractional flow reserve and coronary bifurcation anatomy: a novel quantitative model to assess and report the stenosis severity of bifurcation lesions. JACC Cardiovasc Interv. 2015;8: 564-74.

18. Westra J, Li Z, Rasmussen LD, Winther S, Li G, Nissen L, Petersen SE, Ejlersen JA, Isaksen C, Gormsen LC, Urbonaviciene G, Eftekhari A, Weng T, Qu X, Bøtker HE, Christiansen EH, Holm NR, Bøttcher M, Tu S. One-step anatomic and function testing by cardiac CT versus second-line functional testing in symptomatic patients with coronary artery stenosis: head-to-head comparison of CT-derived fractional flow reserve and myocardial perfusion imaging. EuroIntervention. 2021;17:576-83.

19. Westra J, Sejr-Hansen M, Koltowski L, Mejía-Rentería H, Tu S, Kochman J, Zhang Y, Liu T, Campo G, Hjort J, Mogensen LJH, Erriquez A, Andersen BK, Eftekhari A, Escaned J, Christiansen EH, Holm NR. Reproducibility of quantitative flow ratio: the QREP study. EuroIntervention. 2022;17:1252-9.

20. Johnson NP, Johnson DT, Kirkeeide RL, Berry C, De Bruyne B, Fearon WF, Oldroyd KG, Pijls NHJ, Gould KL. Repeatability of Fractional Flow Reserve Despite Variations in Systemic and Coronary Hemodynamics. JACC Cardiovasc Interv. 2015; 8:1018-27.

21. Hong H, Jia H, Zeng M, Gutierrez-Chico JL, Wang Y, Zeng X, Qin Y, Zhao C, Chu M, Huang J, Liu L, Hu S, He L, Chen L, Wijns W, Yu B, Tu S. Risk Stratification in Acute Coronary Syndrome by Comprehensive Morphofunctional Assessment With Optical Coherence Tomography. JACC Asia. 2022;2:460-72.

22. Yu W, Tanigaki T, Ding D, Wu P, Du H, Ling L, Huang B, Li G, Yang W, Zhang S, Yan F, Okubo M, Xu B, Matsuo H, Wijns W, Tu S. Accuracy of Intravascular Ultrasound-Based Fractional Flow Reserve in Identifying Hemodynamic Significance of Coronary Stenosis. Circ Cardiovasc Interv. 2021;14:e009840.

23. Götberg M, Christiansen EH, Gudmundsdottir IJ, Sandhall L, Danielewicz M, Jakobsen L, Olsson SE, Öhagen P, Olsson H, Omerovic E, Calais F, Lindroos P, Maeng M, Tödt T, Venetsanos D, James SK, Kåregren A, Nilsson M, Carlsson J, Hauer D, Jensen J, Karlsson AC, Panayi G, Erlinge D, Fröbert O; iFR-SWEDEHEART Investigators. Instantaneous Wave-free Ratio versus Fractional Flow Reserve to Guide PCI. N Engl J Med. 2017;376:1813-23.

24. Fearon WF, Zimmermann FM, De Bruyne B, Piroth Z, van Straten AHM, Szekely L, Davidavičius G, Kalinauskas G, Mansour S, Kharbanda R, Östlund-Papadogeorgos N, Aminian A, Oldroyd KG, Al-Attar N, Jagic N, Dambrink JE, Kala P,

Angerås O, MacCarthy P, Wendler O, Casselman F, Witt N, Mavromatis K, Miner SES, Sarma J, Engstrøm T, Christiansen EH, Tonino PAL, Reardon MJ, Lu D, Ding VY, Kobayashi Y, Hlatky MA, Mahaffey KW, Desai M, Woo YJ, Yeung AC, Pijls NHJ; FAME 3 Investigators. Fractional Flow Reserve-Guided PCI as Compared with Coronary Bypass Surgery. *N Engl J Med.* 2022;386:128-37.

25. De Bruyne B, Hersbach F, Pijls NH, Bartunek J, Bech JW, Heyndrickx GR, Gould KL, Wijns W. Abnormal epicardial coronary resistance in patients with diffuse atherosclerosis but "Normal" coronary angiography. *Circulation.* 2001;104:2401-6.

Supplementary data

Supplementary Table 1. Detailed search strategy.

Supplementary Table 2. Concordance correlation coefficient of OFR and FFR.

Supplementary Table 3. Leave-one-out sensitivity analysis of numerical difference of OFR and FFR.

Supplementary Table 4. Vessel-level diagnostic concordance of OFR and FFR in pre- and post-PCI vessels separately.

Supplementary Table 5. Vessel-level diagnostic performance and numerical agreement of OFR against wire-based FFR.

Supplementary Table 6. Patient-level diagnostic performance and numerical agreement of OFR against wire-based FFR.

Supplementary Table 7. Distribution of OFR−FFR ≥0.10 and OFR−FFR ≤−0.10 discrepancy cases by the range of FFR values.

Supplementary Figure 1. Study flowchart.

Supplementary Figure 2. Summary table of risk of bias and applicability concerns.

Supplementary Figure 3. Vessel-level Deek's funnel plot asymmetry test for all 5 included studies.

Supplementary Figure 4. Scatter plots and Bland-Altman plots between OFR and FFR.

Supplementary Figure 5. Estimated mean difference by pooled OFR and FFR data in pre-PCI and post-PCI vessels separately.

Supplementary Figure 6. Estimated mean difference of OFR and FFR between Asian centres and European & American centres.

Supplementary Figure 7. Estimated mean difference of OFR and FFR among centre level in pre- and post-PCI groups separately.

Supplementary Figure 8. Estimated mean difference of OFR and FFR between Asian and European & American centres in pre- and post-PCI groups separately.

Supplementary Figure 9. The distribution of OFR according to ranges of FFR.

Supplementary Figure 10. The pooled diagnostic performance estimation on sensitivity.

Supplementary Figure 11. The pooled diagnostic performance estimation on specificity.

Supplementary Figure 12. The pooled diagnostic performance estimation on PPV.

Supplementary Figure 13. The pooled diagnostic performance estimation on NPV.

Supplementary Figure 14. The pooled diagnostic performance estimation on LR+.

Supplementary Figure 15. The pooled diagnostic performance estimation on LR−.

Supplementary Figure 16. Vessel-level hierarchical summary ROC curve for all 5 included studies.

Supplementary Figure 17. Patient-level hierarchical summary ROC curve for all 5 included studies.

Moving image 1. A representative case example of OFR analysis.

The supplementary data are published online at:
https://eurointervention.pcronline.com/
doi/10.4244/EIJ-D-22-01098

Supplementary data

Supplementary Table 1. Detailed search strategy.

Search		Results
MEDLINE (PubMed)		
("fractional flow reserve" OR "FFR") AND ("OFR" OR "optical flow ratio ")		6
EMBASE		
#9	Search #7 AND #8	10
#8	Search #4 OR #5	791
#7	Search #3 AND #6	713
#6	Search #1 OR #2	10534
#5	Search "OFR"	788
#4	Search "optical flow ratio"	9
#3	Search "optical coherence tomography"	85604
#2	Search "FFR"	6907
#1	Search "fractional flow reserve"	8551
The last search was performed on May 1st 2022		

FFR, fractional flow reserve; OFR, optical flow ratio.

Supplementary Table 2. Concordance correlation coefficient of OFR and FFR.

	Vessel-level					
	One-stage approach			Two-stage approach		
	Pre-PCI	Post-PCI	Combined	Pre-PCI	Post-PCI	Combined
Concordance correlation coefficient (95% CI)	0.81 (0.78,0.84)	0.86 (0.82,0.89)	0.86 (0.84,0.88)	0.85 (0.82,0.87)	0.88 (0.85,0.91)	0.86 (0.84,0.88)
	Patient-level					
	One-stage approach			Two-stage approach		
	Pre-PCI	Post-PCI	Combined	Pre-PCI	Post-PCI	Combined
Concordance correlation coefficient (95% CI)	0.82 (0.78,0.85)	0.86 (0.82,0.89)	0.88 (0.86,0.89)	0.85 (0.82,0.88)	0.88 (0.85,0.91)	0.87 (0.85,0.89)

Supplementary Table 3. Leave-one-out sensitivity analysis of numerical difference of OFR and FFR.

Vessel-level		Patient-level	
Study omitted	OFR-FFR mean difference (95% CI)	Study omitted	OFR-FFR mean difference (95% CI)
Yu et al.	0.013 (-0.111, 0.137)	Yu et al.	0.003 (-0.006, 0.012)
Huang et al.	0.053 (-0.083, 0.189)	Huang et al.	0.004 (-0.006, 0.013)
Chico et al.	0.032 (-0.085, 0.149)	Chico et al.	0.004 (-0.004, 0.013)
Emori et al.	0.017 (-0.105, 0.138)	Emori et al.	0.003 (-0.007, 0.013)
Ding et al.	0.004 (-0.119, 0.127)	Ding et al.	0.002 (-0.009, 0.012)

FFR, fractional flow reserve; OFR, optical flow ratio.

Supplementary Table 4. Vessel-level diagnostic concordance of OFR and FFR in pre- and post-PCI vessels separately.

Pre-PCI vessels			
OFR	**FFR**		**Total**
	≤0.8	**>0.8**	
≤0.8	219	14	233
>0.8	22	149	171
Total	241	163	404
Post-PCI vessels			
OFR	**FFR**		**Total**
	≤0.9	**>0.9**	
≤0.9	128	9	137
>0.9	19	66	85
Total	147	75	222

FFR, fractional flow reserve; OFR, optical flow ratio; PCI, percutaneous coronary

intervention.

Supplementary Table 5. Vessel-level diagnostic performance and numerical agreement of OFR against wire-based FFR.

	One-stage approach			Two-stage approach		
	Pre-PCI	**Post-PCI**	**Combined**	**Pre-PCI**	**Post-PCI**	**Combined**
Accuracy, % (95%CI)	91 (88, 94)	87 (82, 91)	90 (87, 92)	92 (89, 94)	87 (82, 92)	91 (88, 93)
Sensitivity, % (95%CI)	87 (81, 92)	78 (67, 86)	84 (79, 88)	88 (85, 91)	78 (73, 83)	85 (82, 88)
Specificity, % (95%CI)	94 (90, 97)	93 (88, 97)	94 (91, 96)	94 (92, 96)	93 (90, 97)	94 (92, 96)
LR (+), (95%CI)	14.50 (8.70, 24.18)	11.82 (6.22, 22.45)	13.51 (9.06, 20.14)	13.15 (5.34, 20.96)	9.91 (2.34, 17.48)	11.48 (6.04, 16.91)
LR (-), (95%CI)	0.14 (0.09, 0.20)	0.24 (0.16, 0.36)	0.17 (0.13, 0.23)	0.14 (0.08, 0.20)	0.23 (0.14, 0.31)	0.17 (0.12, 0.22)

PPV, % (95%CI)	91 (86, 95)	88 (79, 93)	90 (86, 93)	92 (89, 94)	90 (86, 94)	91 (89, 93)
NPV, % (95%CI)	91 (87, 94)	87 (82, 91)	89 (86, 92)	92 (89, 95)	86 (82, 91)	91 (88, 93)
AUC (95%CI)	0.91 (0.87, 0.93)	0.86 (0.80, 0.90)	0.89 (0.86, 0.91)	0.96 (0.94, 0.98)	0.89 (0.85, 0.94)	0.95 (0.93, 0.97)
Mean difference	-0.001 (-0.006, 0.005)	0.004 (0.000, 0.008)	0.001 (-0.003, 0.005)	-0.001 (-0.014, 0.012)	0.005 (-0.006, 0.015)	0.002 (-0.006, 0.011)

AUC, area under the receiver operating curve; LR (+), positive likelihood ratio; LR (-), negative likelihood ratio; NPV, negative predictive value;
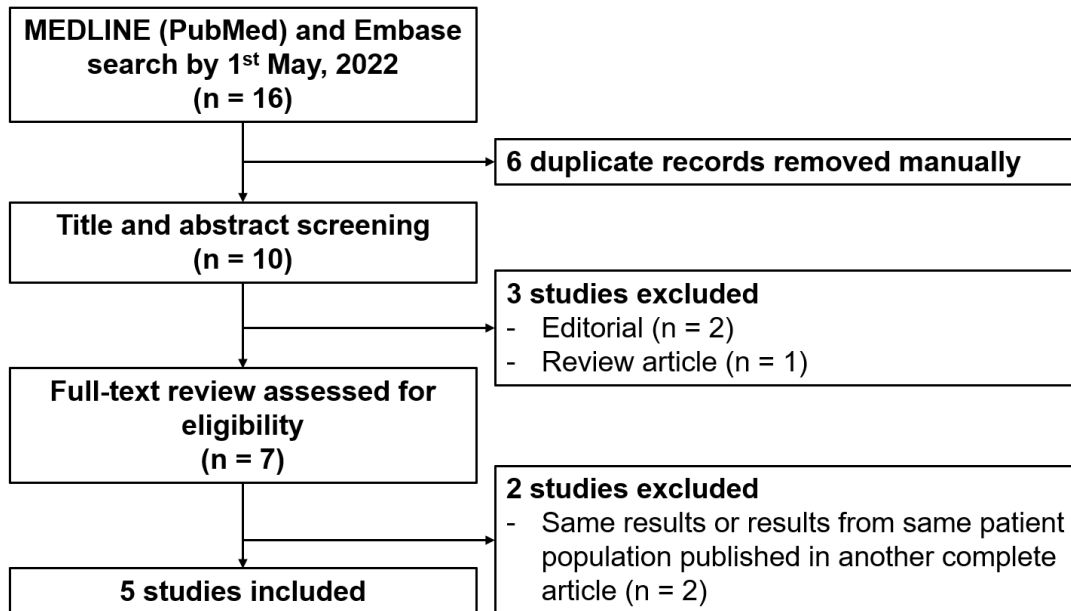
PCI, percutaneous coronary intervention; PPV, positive predictive value.

Supplementary Table 6. Patient-level diagnostic performance and numerical agreement of OFR against wire-based FFR.

	One-stage approach			Two-stage approach		
	Pre-PCI	**Post-PCI**	**Combined**	**Pre-PCI**	**Post-PCI**	**Combined**
Accuracy, % (95%CI)	91 (88, 94)	87 (82, 91)	90 (87, 92)	92 (89, 94)	87 (82, 92)	91 (88, 93)
Sensitivity, % (95%CI)	88 (83, 93)	78 (67, 86)	85 (80, 89)	90 (87, 93)	78 (73, 83)	87 (84, 89)
Specificity, % (95%CI)	94 (90, 97)	93 (88, 97)	94 (91, 96)	94 (92, 97)	93 (90, 97)	94 (92, 96)
LR (+), (95%CI)	15.11 (8.49, 26.88)	11.82 (6.22, 22.45)	13.77 (8.98, 21.12)	14.66 (4.71, 24.60)	9.81 (2.28, 17.34)	11.58 (5.57, 17.58)
LR (-),	0.12 (0.08, 0.19)	0.24 (0.16, 0.36)	0.16 (0.12, 0.22)	0.13 (0.07, 0.18)	0.21 (0.11, 0.30)	0.15 (0.10, 0.20)

(95%CI)						
PPV, % **(95%CI)**	93 (88, 96)	88 (79, 93)	91 (87, 94)	93 (91, 96)	89 (85, 93)	92 (90, 94)
NPV, % **(95%CI)**	90 (86, 93)	87 (82, 91)	89 (86, 92)	92 (90, 95)	87 (83, 91)	91 (89, 93)
AUC **(95%CI)**	0.91 (0.88, 0.94)	0.86 (0.80, 0.90)	0.89 (0.87, 0.92)	0.92 (0.89, 0.95)	0.86 (0.82, 0.91)	0.90 (0.88, 0.93)
Mean difference **(95% CI)**	0.001 (-0.005, 0.007)	0.004 (0.000, 0.008)	0.002 (-0.002, 0.006)	0.001 (-0.013, 0.014)	0.005 (-0.006, 0.015)	0.003 (-0.005, 0.011)

AUC, area under the receiver operating curve; LR (+), positive likelihood ratio; LR (-), negative likelihood ratio; NPV, negative predictive value;

PCI, percutaneous coronary intervention; PPV, positive predictive value

Supplementary Table 7. Distribution of OFR−FFR ≥0.10 and OFR−FFR ≤ −0.10 discrepancy cases by the range of FFR values

		Vessel-level					
FFR Range	**Total number of vessels**	**OFR-FFR ≥0.10**			**OFR-FFR ≤-0.10**		
	Pre-/Post-	Combined	Pre-PCI	Post-PCI	Combined	Pre-PCI	Post-PCI
≤ 0.6	4/0	3	3	0	0	0	0
(0.6, 0.7)	45/0	7	7	0	1	1	0
[0.7,0.8)	107/8	5	5	0	8	8	0
[0.8,0.9)	156/70	5	4	1	6	5	1
[0.9, 1.0]	92/144	0	0	0	8	8	0
In total	404/222	20	19	1	23	22	1
		Patient-level					
FFR Range	**Total number of vessels**	**OFR-FFR ≥0.10**			**OFR-FFR ≤-0.10**		
	Pre-/Post-	Combined	Pre-PCI	Post-PCI	Combined	Pre-PCI	Post-PCI
≤ 0.6	4/0	3	3	0	0	0	0
(0.6, 0.7)	45/0	7	7	0	1	1	0
[0.7,0.8)	101/8	2	2	0	8	8	0
[0.8,0.9)	139/70	5	4	1	4	3	1
[0.9, 1.0]	63/144	0	0	0	4	4	0
In total	352/222	17	16	1	17	16	1

FFR, fractional flow reserve; OFR, optical flow ratio.

```
┌─────────────────────────────────┐
│  MEDLINE (PubMed) and Embase    │
│    search by 1st May, 2022      │
│           (n = 16)              │
└─────────────────────────────────┘
         │
         │          ┌──────────────────────────────────────┐
         ├─────────▶│ 6 duplicate records removed manually │
         │          └──────────────────────────────────────┘
         ▼
┌─────────────────────────────────┐
│  Title and abstract screening   │
│           (n = 10)              │
└─────────────────────────────────┘
         │          ┌──────────────────────────────────────┐
         │          │ 3 studies excluded                   │
         ├─────────▶│ -  Editorial (n = 2)                 │
         │          │ -  Review article (n = 1)            │
         ▼          └──────────────────────────────────────┘
┌─────────────────────────────────┐
│  Full-text review assessed for  │
│           eligibility           │
│           (n = 7)               │
└─────────────────────────────────┘
         │          ┌──────────────────────────────────────┐
         │          │ 2 studies excluded                   │
         │          │ -  Same results or results from same │
         ├─────────▶│    patient population published in   │
         │          │    another complete article (n = 2)  │
         ▼          └──────────────────────────────────────┘
┌─────────────────────────────────┐
│      5 studies included         │
└─────────────────────────────────┘
```

Supplementary Figure 1. Study flowchart.

A total of 5 studies were finally included into the current meta-analysis. All included studies provided individual patient-data for this meta-analysis.

Supplementary Figure 2. Summary table of risk of bias and applicability concerns.

All 5 included studies showed high methodological quality with low risk of bias rated
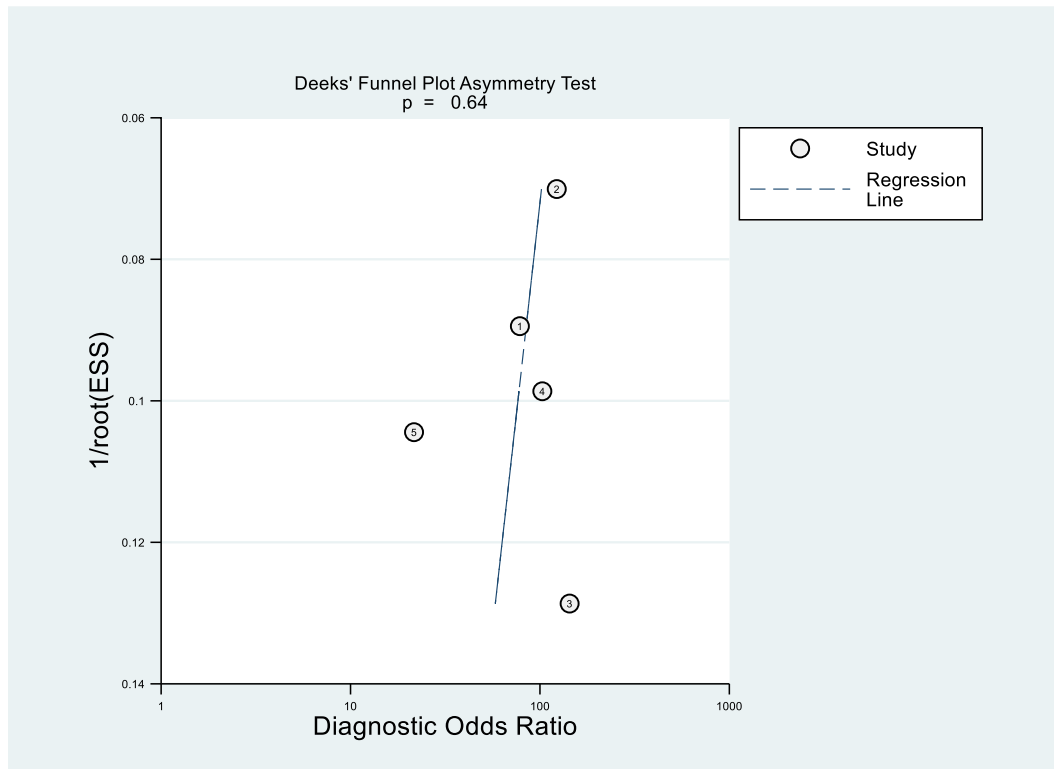
by QUADAS-2.

Supplementary Figure 3. Vessel-level Deek's funnel plot asymmetry test for all 5

included studies.

Each of the five included studies is represented by a datapoint (hollowed circle in the

plot) with paired diagnostic odds ratio – inverse of square root of effective sample

size. The studies are indicated by numbers in the circle: 1 for Yu et al.; 2 for Huang et

al.; 3 for Chico et al.; 4 for Emori et al.; and 5 for Ding et al. Deek's funnel plot

asymmetry test showed that there was no significant publication bias (p = 0.64).

ESS, effective sample size.
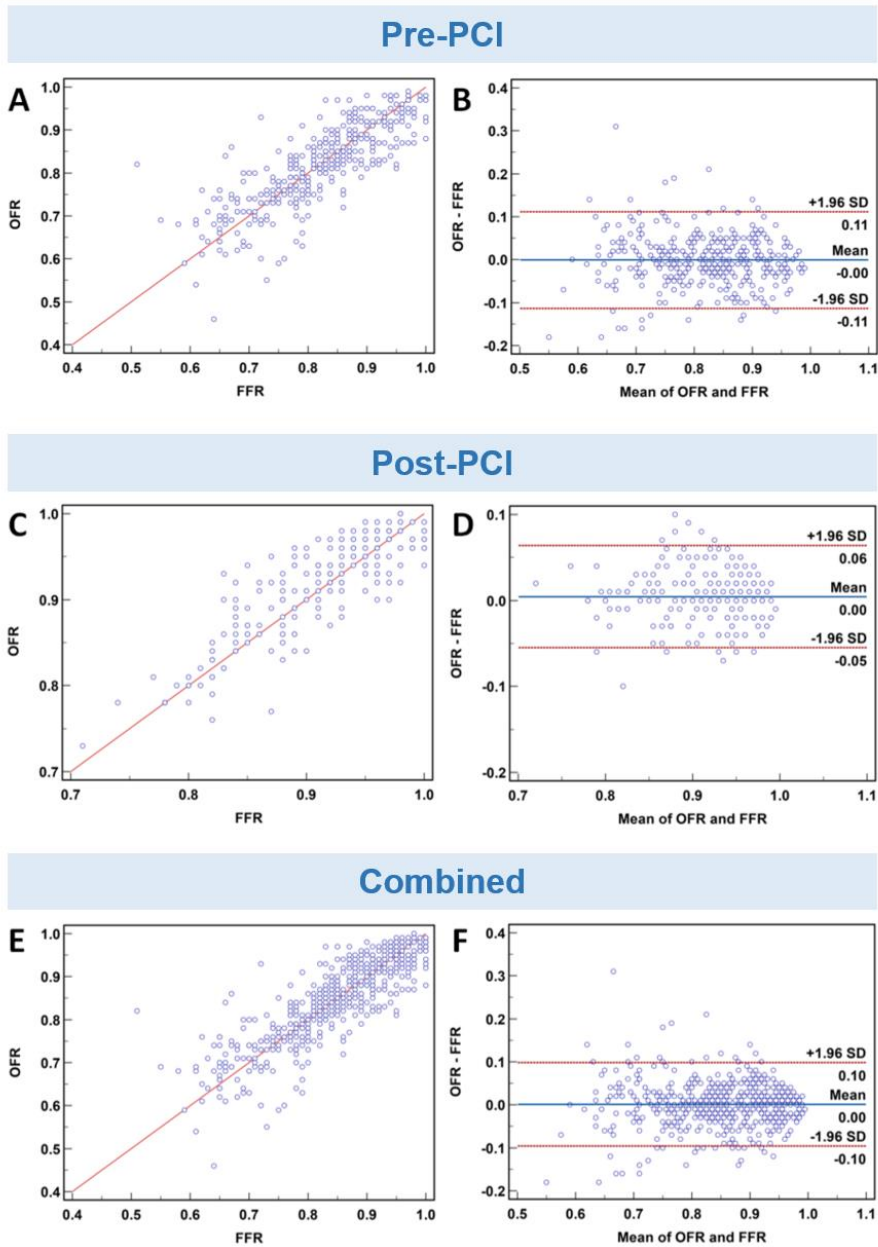
Supplementary Figure 4. Scatter plots and Bland-Altman plots between OFR and FFR.

OFR and FFR showed good correlation and agreement in pre-PCI vessels only (A, B),

post-PCI vessels only (C, D), and in combined vessels (E, F).

FFR, fractional flow reserve; OFR, optical flow ratio; PCI, percutaneous coronary

intervention.
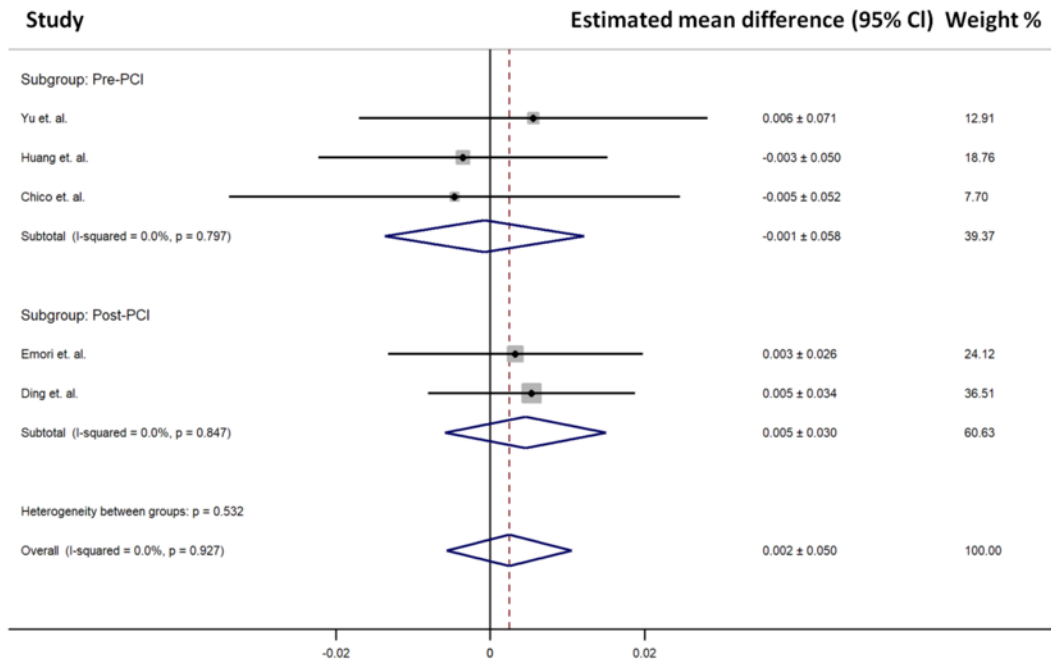
Supplementary Figure 5. Estimated mean difference by pooled OFR and FFR data in pre-PCI and post-PCI vessels separately.

Pooled forest plot showed that the mean difference of OFR and FFR was low in either pre- or post-PCI vessels.

FFR, fractional flow reserve; OFR, optical flow ratio; PCI, percutaneous coronary intervention.
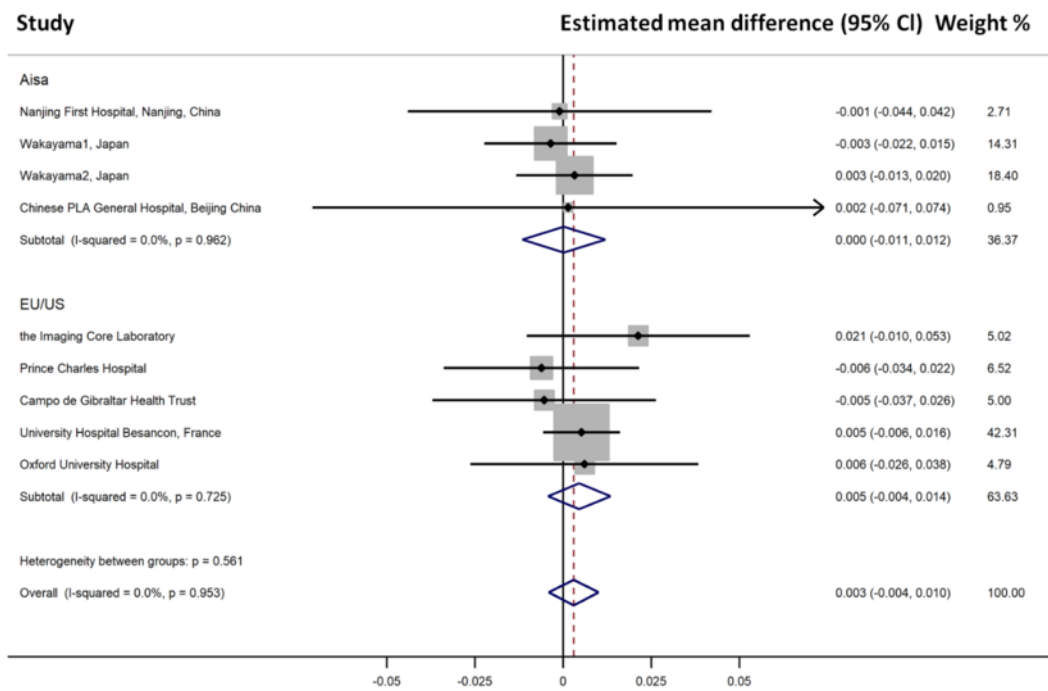
Supplementary Figure 6. Estimated mean difference of OFR and FFR between Asian centres and European & American centres.

Forest plot showed that the mean difference of OFR and FFR was not significantly different in Asia centers or in European & American centers.

Wakayama1: the data from Huang et. al. Wakayama2: the data from Emori et. al.

FFR, fractional flow reserve; OFR, optical flow ratio; PCI, percutaneous coronary intervention.
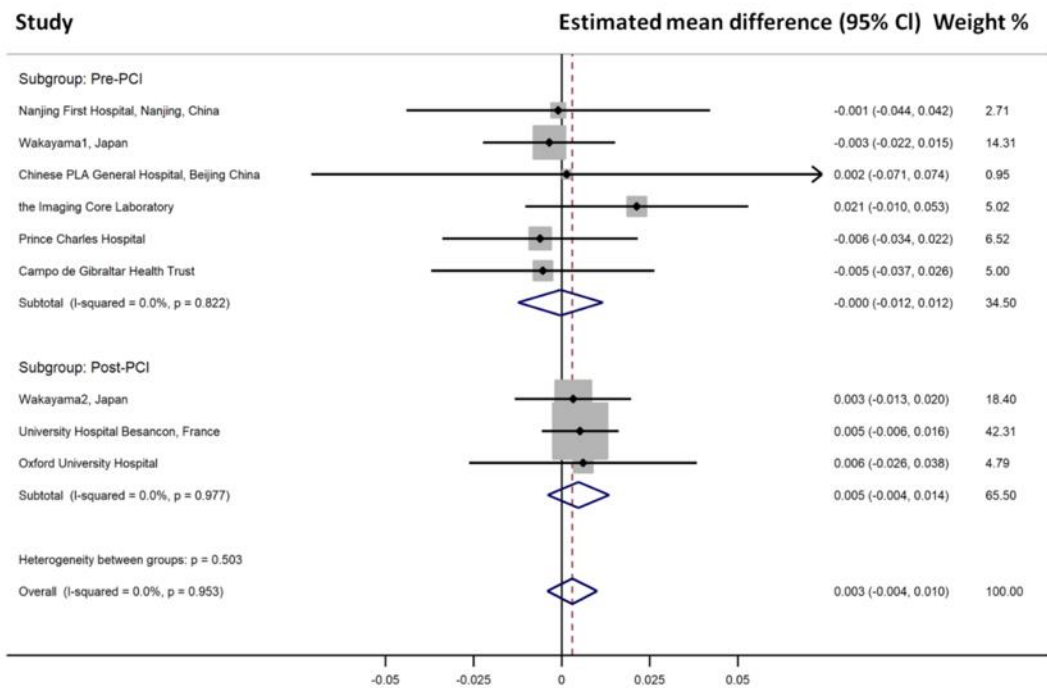
Supplementary Figure 7. Estimated mean difference of OFR and FFR among centre level in pre- and post-PCI groups separately.

Forest plot pooled by centre level accounts for no significant statistical difference over centers.

Wakayama1: the data from Huang et. al. Wakayama2: the data from Emori et. al.

FFR, fractional flow reserve; OFR, optical flow ratio; PCI, percutaneous coronary intervention.
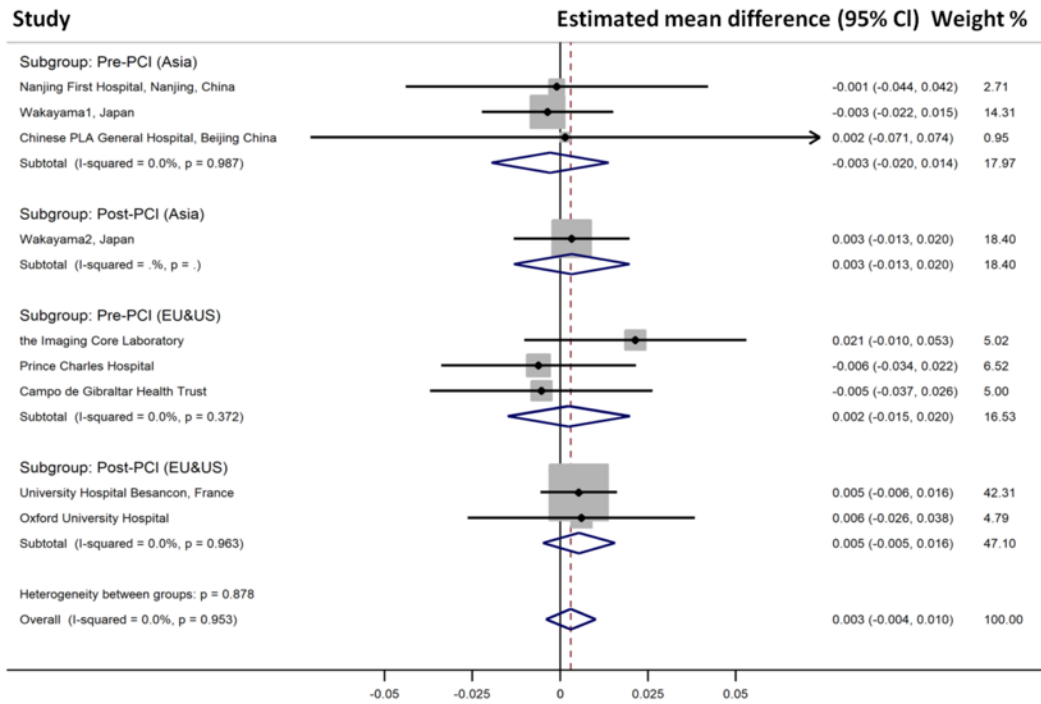
Supplementary Figure 8. Estimated mean difference of OFR and FFR between Asian

and European & American centres in pre- and post-PCI groups separately.

Forest plot pooled by centre level accounts for no significant statistical difference over

regions.

Wakayama1: the data from Huang et. al. Wakayama2: the data from Emori et. al.

FFR, fractional flow reserve; OFR, optical flow ratio; PCI, percutaneous coronary

intervention.
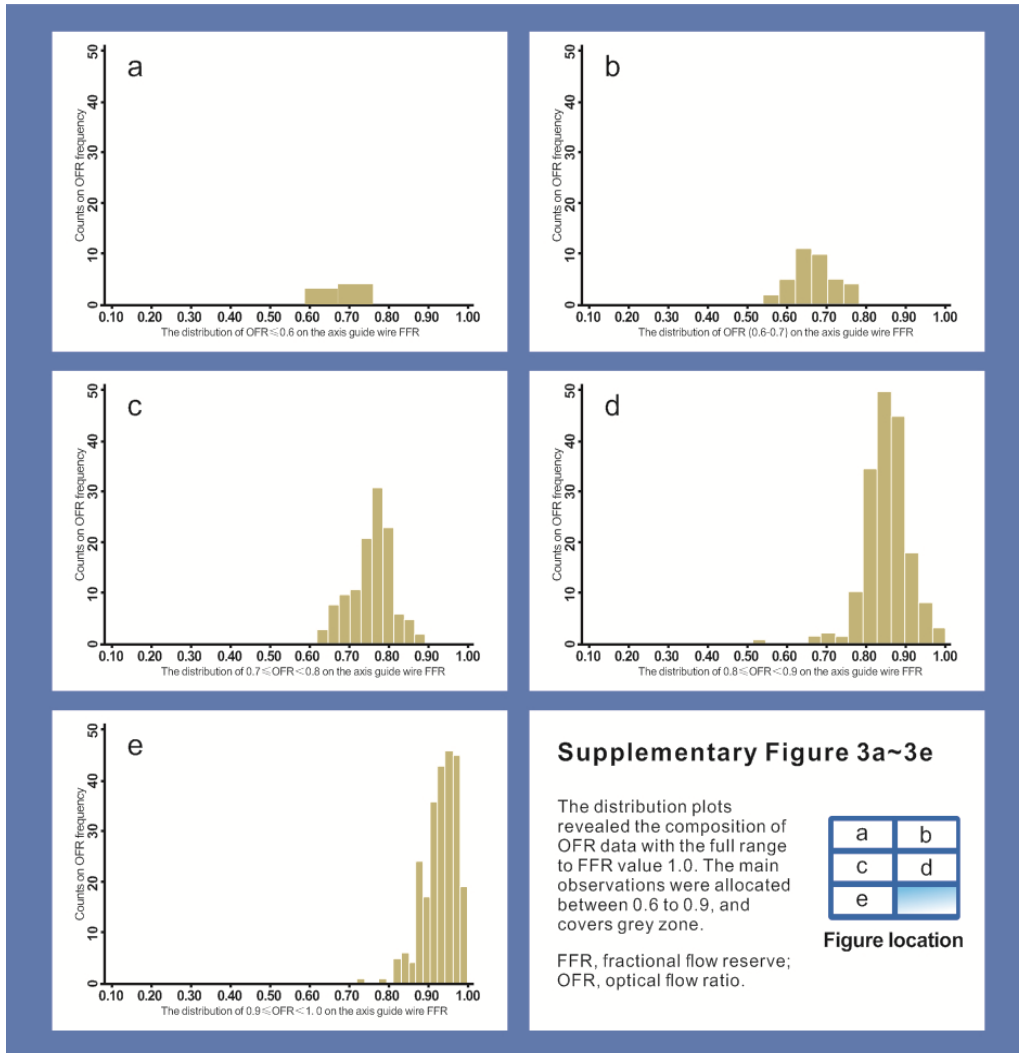
Supplementary Figure 9. The distribution of OFR according to ranges of FFR.

FFR, fractional flow reserve; OFR, optical flow ratio.
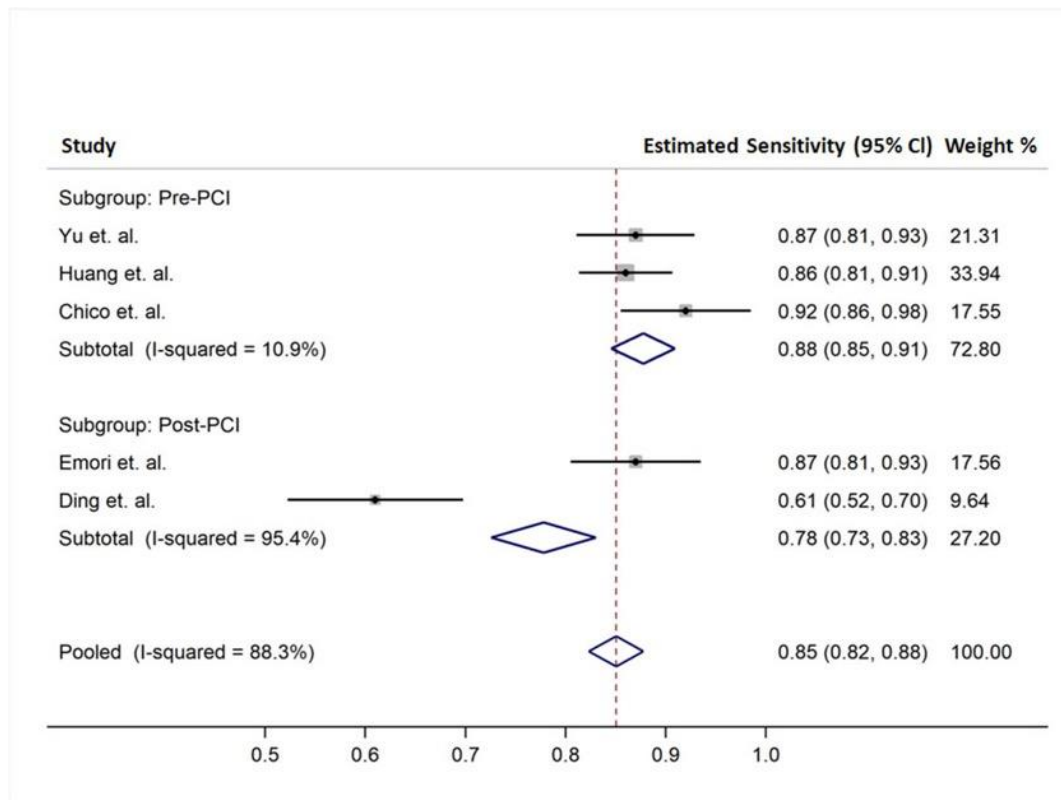
Supplementary Figure 10. The pooled diagnostic performance estimation on

sensitivity.

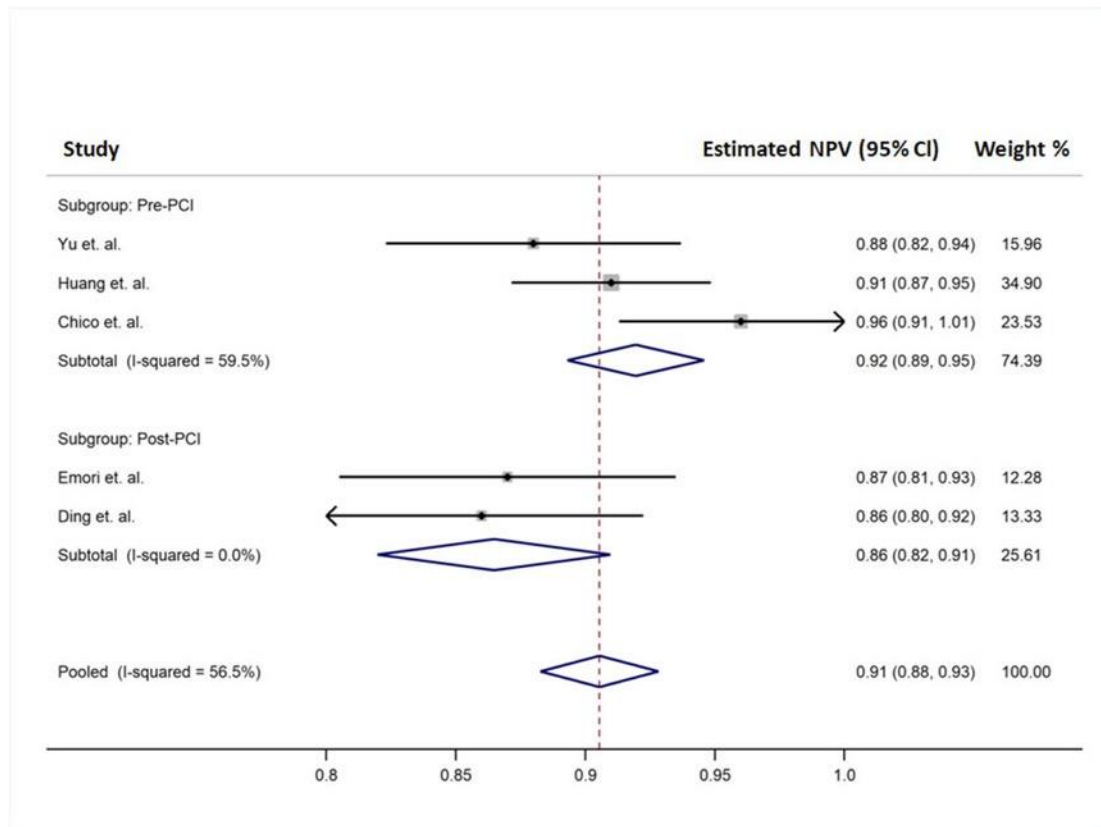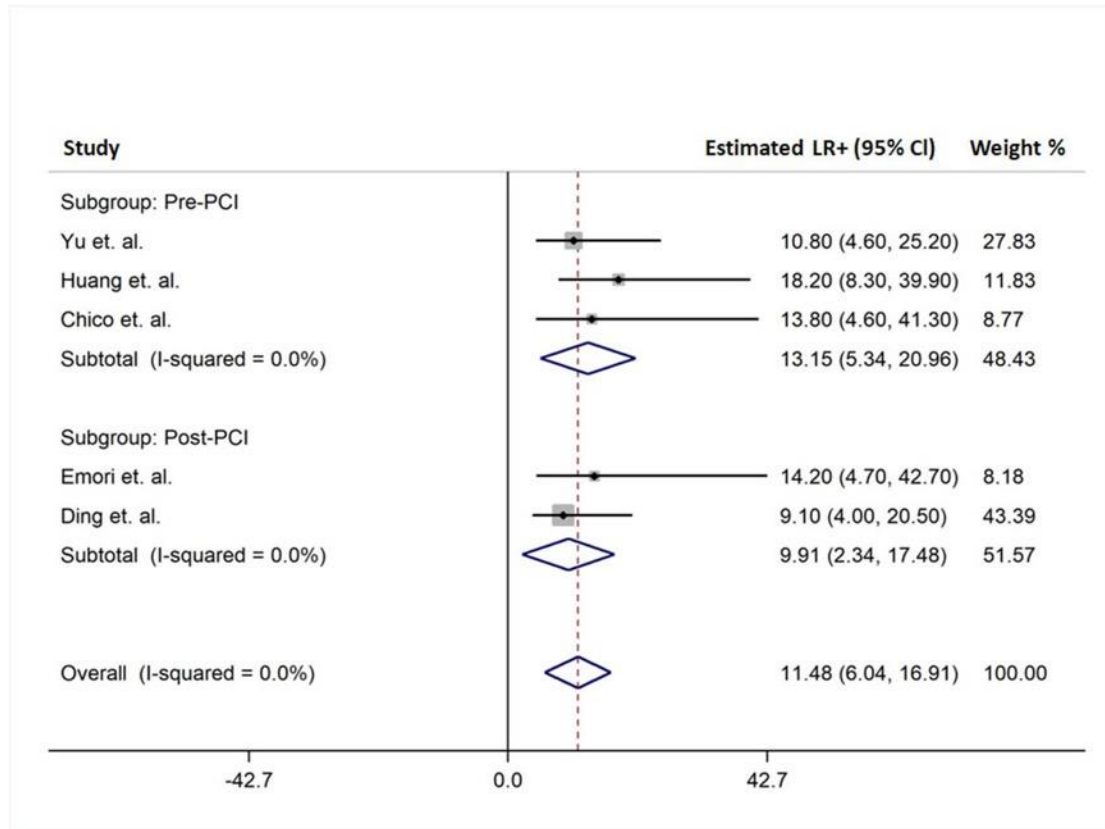Pooled overall sensitivity was 85% (95%Cl 82%-88%, $I^2 = 88.3\%$).

PCI, percutaneous coronary intervention.
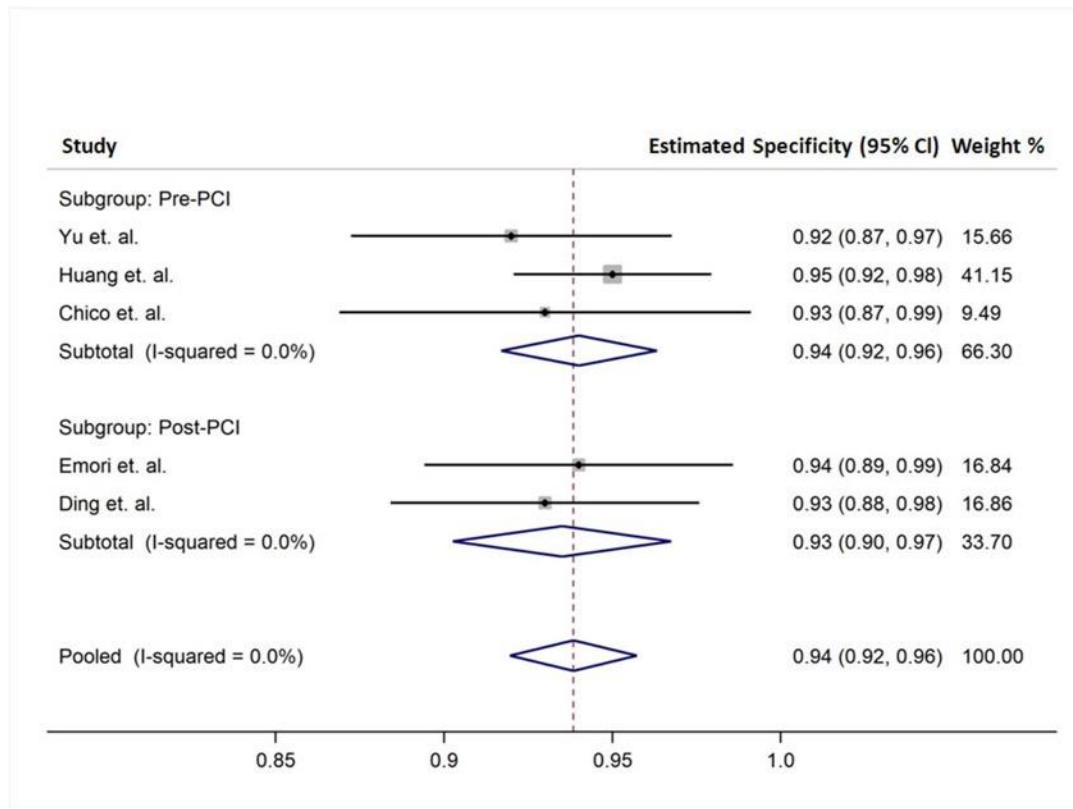
Supplementary Figure 11. The pooled diagnostic performance estimation on

specificity.

Pooled overall specificity was 94% (95%Cl 92%-96%, $I^2 = 0.0\%$).

PCI, percutaneous coronary intervention.
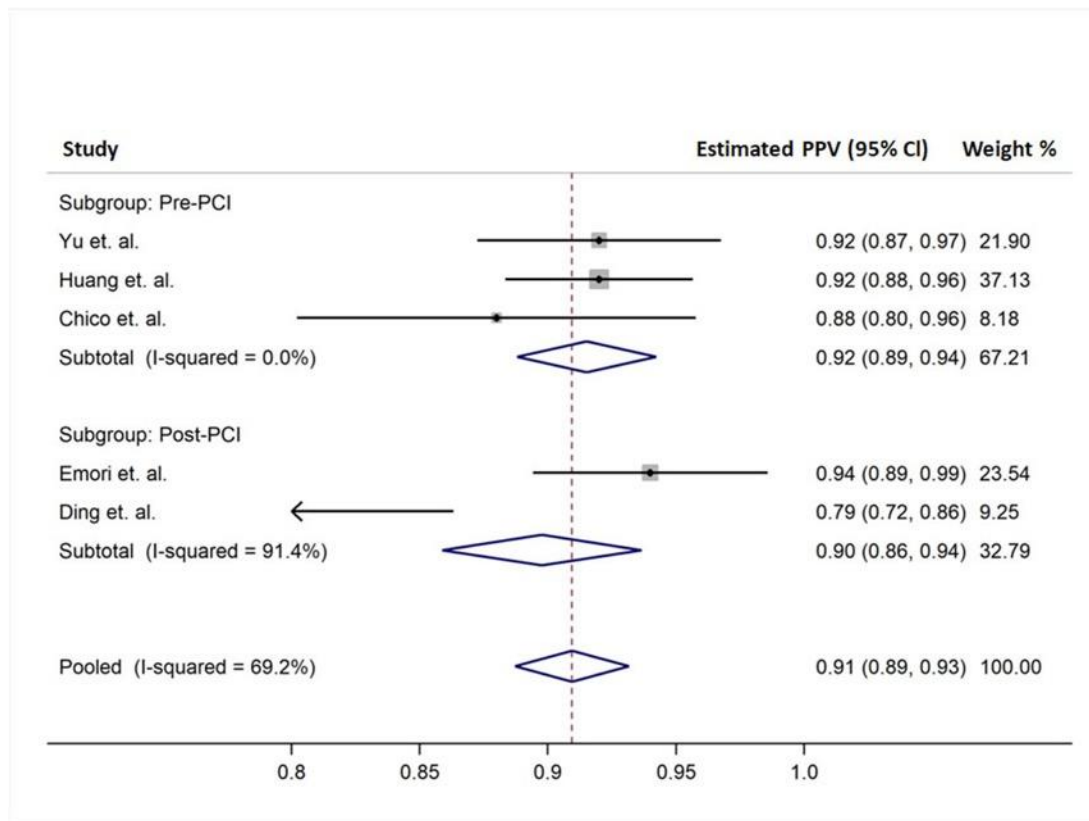
Supplementary Figure 12. The pooled diagnostic performance estimation on PPV.
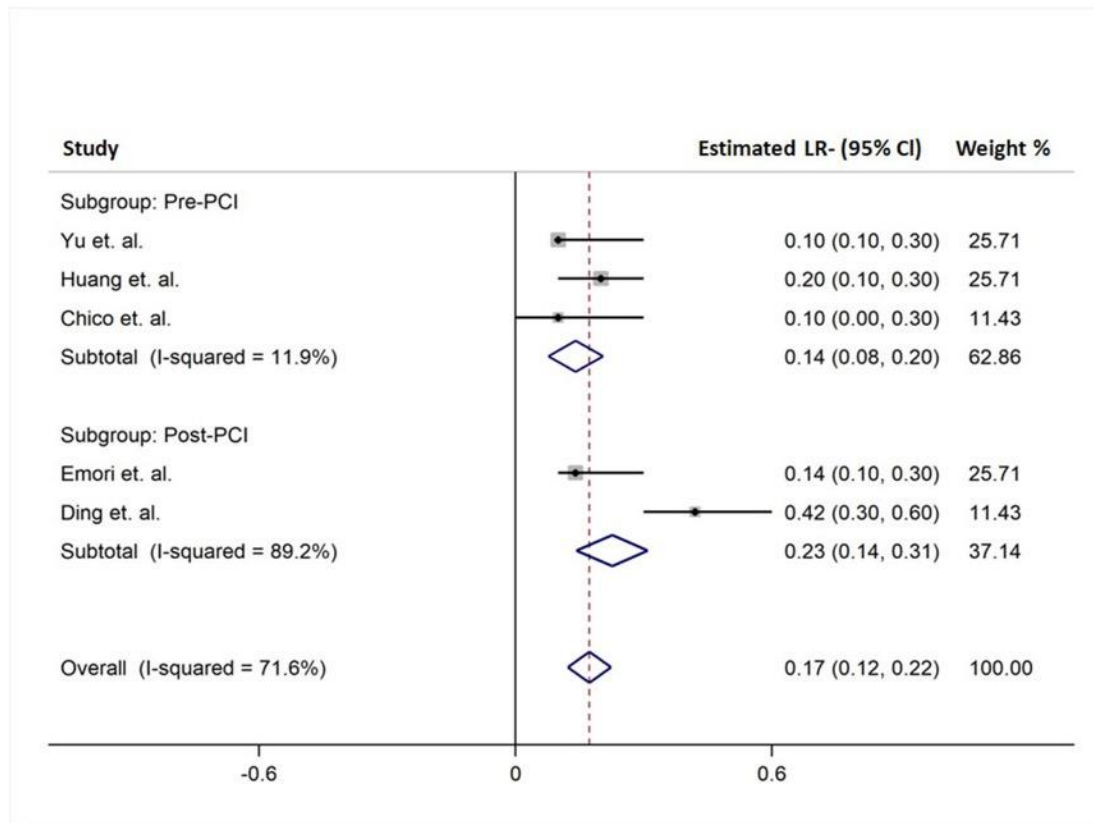
Pooled overall PPV was 91% (95%Cl 89%-93%, I^2 = 69.2%).

PCI, percutaneous coronary intervention; PPV, positive predictive value.

Supplementary Figure 13. The pooled diagnostic performance estimation on NPV.

Pooled overall NPV was 91% (95%Cl 88%-93%, I^2 = 56.5%).

NPV, negative predictive value; PCI, percutaneous coronary intervention.

Supplementary Figure 14. The pooled diagnostic performance estimation on LR+.

Pooled overall positive likelihood ratio was 11.48 (95%CI 6.04-16.91, $I^2 = 0.0\%$).

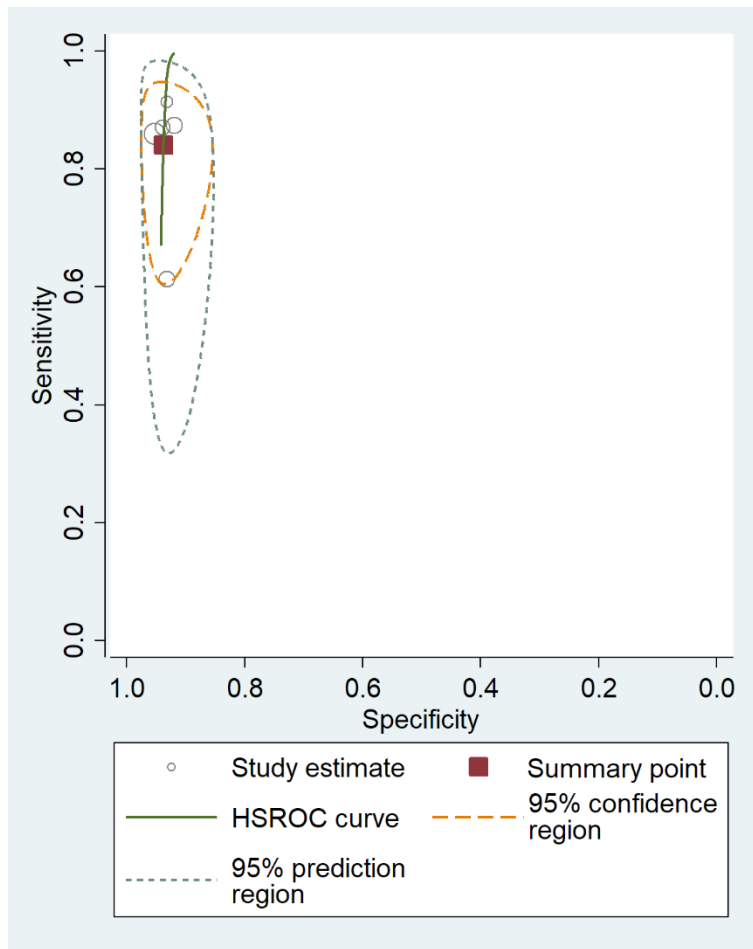LR (+), positive likelihood ratio; PCI, percutaneous coronary intervention.

Supplementary Figure 15. The pooled diagnostic performance estimation on LR−.

Pooled overall negative likelihood ratio was 0.17 (95%CI 0.12-0.22, $I^2 = 71.6\%$).
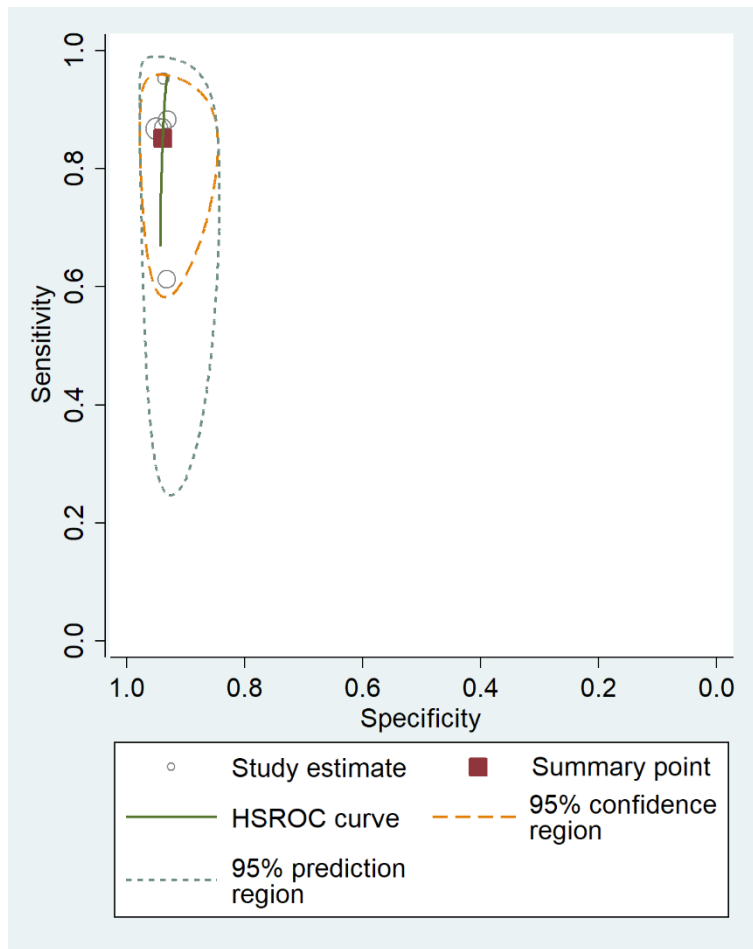
LR (-), negative likelihood ratio; PCI, percutaneous coronary intervention.

Supplementary Figure 16. Vessel-level hierarchical summary ROC curve for all 5 included studies.

HSROC, hierarchical summary ROC curve.

Supplementary Figure 17. Patient-level hierarchical summary ROC curve for all 5 included studies.

HSROC, hierarchical summary ROC curve.